

Review

Hydrogenation of CO₂ to Olefins over Iron-Based Catalysts: A Review

Wenqi Liu ¹, Sifan Cheng ¹, Haripal Singh Malhi ¹, Xinhua Gao ² , Zhenzhou Zhang ^{1,*} and Weifeng Tu ^{1,*}

¹ Engineering Research Center of Advanced Functional Material Manufacturing of Ministry of Education, School of Chemical Engineering, Zhengzhou University, Zhengzhou 450001, China

² State Key Laboratory of High-Efficiency Utilization of Coal and Green Chemical Engineering, College of Chemistry & Chemical Engineering, Ningxia University, Yinchuan 750014, China

* Correspondence: zhangzhenzhou@zzu.edu.cn (Z.Z.); weifengt@zzu.edu.cn (W.T.)

Abstract: The widespread use of fossil fuels has caused high CO₂ concentrations in the atmosphere, which have had a great impact on climate and the environment. Methods for efficiently utilizing CO₂ to produce high value-added chemicals have received increasing attention. Among the products of CO₂ hydrogenation, olefins, an important petrochemical feedstock, are one of the essential target products. Therefore, CO₂ hydrogenation to olefins has been extensively studied, especially for the development of high-performance catalysts. Iron-based catalysts, which are widely used in Fischer-Tropsch synthesis reactions, have also been considered attractive for use in the CO₂ hydrogenation to olefins due to their excellent performance in catalytic activity and reaction stability. Most studies have focused on the modulation of morphology; reduction and adsorption properties by tuning the methods of catalyst syntheses; pretreatment conditions and the composition of catalysts, in order to improve hydrogenation activity and olefin yield. In this review, we briefly discuss a thermodynamic overview of the CO₂ hydrogenation to olefins reaction, the optimization of catalyst modifications, and current insights into the reaction mechanism; moreover, we summarize current challenges and future trends in the CO₂ hydrogenation to olefins.



Citation: Liu, W.; Cheng, S.; Malhi, H.S.; Gao, X.; Zhang, Z.; Tu, W.

Hydrogenation of CO₂ to Olefins over Iron-Based Catalysts: A Review. *Catalysts* **2022**, *12*, 1432. <https://doi.org/10.3390/catal12111432>

Academic Editor: Giuseppe Bonura

Received: 19 October 2022

Accepted: 11 November 2022

Published: 14 November 2022

Publisher's Note: MDPI stays neutral with regard to jurisdictional claims in published maps and institutional affiliations.



Copyright: © 2022 by the authors. Licensee MDPI, Basel, Switzerland. This article is an open access article distributed under the terms and conditions of the Creative Commons Attribution (CC BY) license (<https://creativecommons.org/licenses/by/4.0/>).

Keywords: carbon dioxide; hydrogenation; olefins; iron-based catalysts

1. Introduction

Global CO₂ emissions from the combustion of fossil fuels and industrial processes reached their highest level of 36.3 gigatons (Gt) in 2021, as shown in Figure 1; this was almost an increase of 6% compared to 2020 [1]. The widespread use of fossil fuels has led to a continuous increase in the atmospheric CO₂ concentration, which reached 417.19 ppm in 2022, 1.51 times higher than that of 277.0 ppm at the beginning of the industrial era in 1750 [2]. It is expected to reach 560 ppm by the end of this century. As a major greenhouse gas, CO₂ causes various environmental problems, such as climate warming [3]. The global surface temperature in 2021 was +1.12 °C higher relative to the 1880–1920 average in the GISS (Goddard Institute for Space Studies) analysis, and the eight warmest years on the record occurred in the past eight years; 2023 may set a new record [2]. However, since fossil fuels will remain the dominant source of energy for decades. It will be challenging to meet the goal of reducing CO₂ emissions, even if we commit to improving energy efficiency and developing uses of renewable energy [4]. Therefore, approaches that utilize CO₂ to create economic value have received a lot of attention [5–8]. Carbon capture and storage (CCS) has been considered the most effective technology [5,9,10] among the different climate change mitigation policies. However, it still faces several technical and economic barriers that must be overcome before it can be deployed on a global scale [11]. Hence, carbon utilization has drawn attention, because it involves the conversion of waste CO₂ emissions into value-added products. CO₂ has been used in various industries, such as food, agrochemicals, welding, foaming, fire extinguishers, propellants, etc. However, there is still a substantial

market demand for developing technologies for the large-scale utilization and conversion of CO₂. Therefore, the conversion of CO₂ into chemicals and energy products offers a promising pathway that has been extensively investigated.

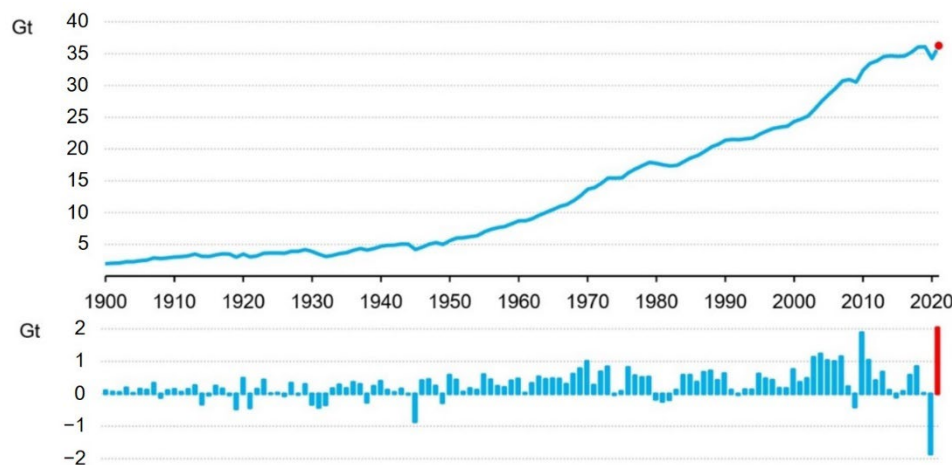


Figure 1. Total CO₂ emissions from energy combustion and industrial processes and their annual change, 1900–2021. Reprinted with permission from ref. [1]. Copyright 2022 IEA.

Thermodynamically, CO₂ is stable, and energy is the basis for its conversion and utilization. As a high-energy material, catalytic CO₂ hydrogenation that uses hydrogen generated from renewable energy sources, such as solar and wind, is an attractive way to achieve this conversion [7,12,13]. A wide variety of CO₂ hydrogenation products can be produced with catalysts containing different active metals, including methane, formic acid and formate, hydrocarbons (especially olefins), alcohols and fuel oils [14,15]. Among the CO₂ conversion pathways, CO₂ hydrogenation to olefins is considered to be an important strategy for the synthesis of carbon-based fuels and feedstocks.

Olefins play a vital role in the petrochemical industry. As the most demanded chemical feedstock, olefins are not only abundant in downstream derivatives, including plastics, synthetic textiles, lubricants, detergents, solvents and cosmetics [16,17], they are also an important component of liquid fossil fuels, such as gasoline, diesel and jet fuel [18–20]. With continuing research on the reaction of CO₂ hydrogenation to olefins, there are two generally accepted reaction pathways: (1) the methanol-to-olefins (MTO) pathway: hydrogenation of CO₂ to methanol followed by the dehydration of methanol to form olefins [21–24]; (2) the direct conversion of CO₂ pathway: hydrogenation of CO₂ to CO via a reverse water-gas-shift (RWGS) reaction, followed by hydrogenation of CO via the classical Fischer–Tropsch synthesis (FTS) reaction to produce olefins. The MTO route usually leads to higher olefin selectivity, because it is not limited by the ASF distribution [25]. However, the temperature regimes for converting CO₂ to methanol and methanol to olefins are different [26]. Methanol to olefins is thermodynamically favorable at high temperatures (400–450 °C), but CO₂ hydrogenation at high temperatures favors CO formation via the RWGS reaction and not methanol [25,27]. Thus, for the MTO route, the low temperature kinetic limitations and high temperature thermodynamic limitations reduce the productivity of methanol and olefins [28]. For the direct conversion of CO₂ pathway, CO formed via the RWGS reaction plays an important role in the downstream FTS process for the target olefin products. The RWGS reaction is endothermic, while the FTS reaction is exothermic, which makes CO₂-FTS thermodynamically more favorable than the RWGS reaction alone [29]. In this review, we focus on the research progress of CO₂ direct hydrogenation to the olefin pathway.

Since the direct CO₂ hydrogenation route shares a common reaction step with the FTS reaction, a similar strategy has been adopted for catalyst design [30–32]. The Fe-based and Co-based catalysts that are commonly used for FTS reaction were also investigated for the CO₂ hydrogenation reaction. Co-based catalysts limit the growth of carbon chains

due to their low RWGS activity and strong adsorption of CO [33,34], resulting in the CO₂ hydrogenation products being mainly methane. Even with the addition of promoters that can promote the RWGS reaction, the lower CO concentration on the catalyst surface makes it difficult to build up the FTS system [35]. Fe-based catalysts with high RWGS and FTS activity and reaction stability have been widely investigated. Usually, the product distribution of CO₂ hydrogenation over Fe-based catalysts follows the Anderson–Schulz–Flory (ASF) law [36]. In order to synthesize the desired products, the ASF distribution limitation must be broken. Currently, most studies have focused on the modulation of morphology, crystal structure, reduction and adsorption properties of Fe-based catalysts, by tuning the methods of catalyst synthesis [37], roasting temperatures [38], pretreatment conditions [39–41] and support materials [42–46], to improve hydrogenation reaction activity and olefin selectivity. In addition, it was found that the doping of auxiliary substances could modulate the surface interface structure of Fe-based catalysts to obtain better catalytic activity and selectivity toward olefins.

2. Thermodynamic Analysis of CO₂ Hydrogenation

The direct hydrogenation of CO₂ is usually considered to be composed of two steps: RWGS reaction to form CO and H₂O, followed by the FTS reaction to generate hydrocarbons [47–49]. Yao et al. [50] conducted a thermodynamic study of a CO₂ hydrogenation system with high olefin selectivity, and assumed that the main products were light olefins and the formation of alkanes was negligible. The enthalpy and Gibbs free energy changes of related reactions at different temperatures are shown in Figure 2. The Δ_rH of the RWGS reaction is greater than 0 at the temperature range from 373.15 K to 1273.15 K, and the Δ_rG decreases with an increase in the temperature, which means the RWGS is an endothermic reaction and prefers a higher temperature. On the contrary, the Δ_rH of the FTS reaction is less than 0, and is the same as the Δ_rG below 650 K. As the temperature increases, Δ_rG of the FTS reaction gradually increases and accelerates with an increase in the carbon number in the products, which means that the lower temperature is in favor of the exothermic FTS reaction, and the formation of higher olefins.

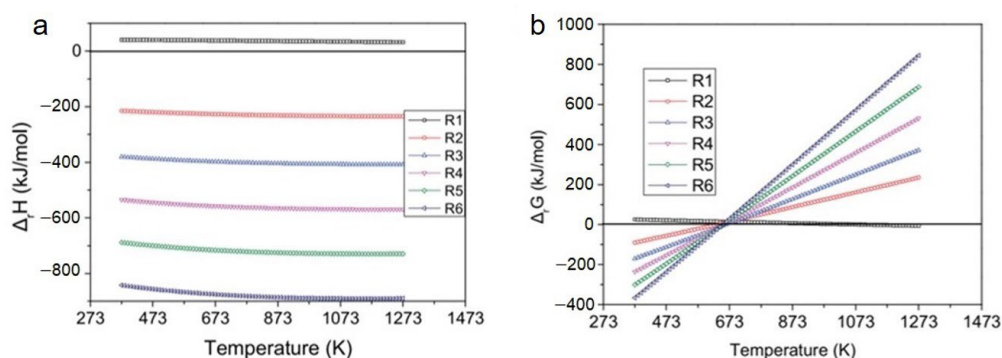


Figure 2. The (a) Δ_rH and (b) Δ_rG of related reactions (R1 represents the RWGS reaction: $\text{CO}_2 + \text{H}_2 \leftrightarrow \text{CO} + \text{H}_2\text{O}$; R2–R6 represents the reaction of $n\text{CO} + 2n\text{H}_2 \rightarrow \text{C}_n\text{H}_{2n} + n\text{H}_2\text{O}$, $n = 2, 3, 4, 5, 6$). Reprinted with permission from ref. [50]. Copyright 2017 Wiley.

In order to simplify the calculation, Liu et al. [51] assumed that the concentration of CO in the system was approximately zero; the reaction mixture was treated as an ideal gas solution, and the hydrocarbon reaction products were low-carbon hydrocarbons (C₁–C₄). The thermodynamic calculations show that the theoretical maximum conversion of CO₂ is 69–71% at a reaction temperature of 580–630 K, a pressure of 2.5–3.0 MPa, and with an H₂/CO₂ ratio of 3. However, the concentration of CO is not zero in the actual reaction system, and the simplified assumption brings a non-negligible effect on the calculation results. Therefore, Liang et al. [17] investigated the thermodynamic equilibrium of CO₂ hydrogenation by considering the concentration of intermediate product CO. The intersection points of ΔG curves for olefins generation are near 320 °C, which is about 40 °C

higher than that for alkanes, and the ΔG for olefins generation is already greater than zero at 320 °C. That is, the yield of alkanes will be greater than the yield of olefins in a reaction system that reaches thermodynamic equilibrium. Therefore, to improve the yield of olefins in the product, the operating conditions and catalysts design should be optimized from the kinetic direction [52].

3. Modification of Catalysts

As mentioned above, the CO_2 hydrogenation reaction is composed of the RWGS reaction followed by the FTS reaction. The conventional Fe-based and Co-based FTS catalysts are generally considered to be suitable for CO_2 hydrogenation as well. Compared with Co, Fe possesses stronger RWGS activity, and thus has higher catalytic activity in the reaction of CO_2 hydrogenation to hydrocarbons [53]. To promote CO_2 conversion and olefin selectivity, various strategies have been used to control the morphology, crystal and electronic structures, and redox properties of Fe-based catalysts [18,35,47,54–60]. The catalytic activity of various Fe-based catalysts reported recently are summarized in Table 1.

Table 1. Summation of Fe-based catalysts used for CO_2 hydrogenation to olefins.

Catalysts	CO ₂ Con. (%)	CO Sel. (%)	Selectivity of Hydrocarbons				O/P	Reaction Conditions			Ref.
			CH ₄	C ₂ ⁰ –C ₄ ⁰	C ₂ ⁼ –C ₄ ⁼	C ₅ ⁺		GHSV (mLg ⁻¹ h ⁻¹)	Temp. (°C)	P (Mpa)	
Fe ₂ O ₃	4.9	3.1 ^b	43.0 ^b	14.1 ^b	25.7 ^b	14.1 ^b	1.8	30,000	330	2.5	[61]
Fe ₃ O ₄ -NaAc	30.4	18.5 ^a	12.0 ^b	4.5 ^b	29.3 ^b	54.2 ^b	6.5	560 ^c	320	0.5	[62]
0.5Na/Fe	35.3	13.2 ^a	31.8 ^b	C ₂ ⁰ –C ₇ ⁰ 10.1 ^b	C ₂ ⁼ –C ₇ ⁼ 57.0 ^b	C ₈ ⁺ 1.2 ^b	5.7	10,000	290	1.5	[63]
FeNa (1.18)	40.5	13.5 ^a	15.8 ^b	7.5 ^b	46.6 ^b	30.1 ^b	6.2	2000	320	3.0	[64]
0.05MnFe	30.0	7.7 ^a	29.3 ^b		C ₂ –C ₅ 63.2 ^b	C ₆ ⁺ 3.9 ^b	0.4	6000	340	2.0	[65]
FeMnNa	35.0	18.1 ^b	10.7 ^b		C ₂ –C ₄ 31.7 ^b	39.5 ^b	8.1	12,000	340	2.0	[66]
Na-Fe ₂ Zn1	43.5	9.2 ^b	11.5 ^b		C ₂ ⁼ –C ₂₀ ⁼ 77.3 ^b		-	15,000	330	1.5	[67]
Na-Fe-Zn	38.0	15.0 ^a	13.0 ^b	C ₂ ⁰ –C ₁₂ ⁰ 9.1 ^b	C ₂ ⁼ –C ₁₂ ⁼ 78.0 ^b	-	8.5	15,000	340	2.5	[68]
Fe-Zn-2Na	43.0	15.7 ^b	22.8 ^b	7.4 ^b	54.1 ^b	-	7.3	10,000	320	1.5	[69]
FeK/MPC	50.6	8.2 ^b	15.4 ^b		C ₂ –C ₄ 31.9 ^b	44.5 ^b	-	2000	300	2.5	[45]
Fe ₂ O ₃ -CT600	23.0	21.0 ^c	14.0 ^a		C ₂ ⁺ 65.0 ^a		1.4	1140 ^c	300	1.0	[48]
Na-Fe ₃ O ₄ /HZSM-5	22.0	20.1 ^a	4.0 ^b		C ₂ –C ₄ 16.6 ^b	79.4 ^b	-	4000	320	3.0	[70]
15Fe-K/m-ZrO ₂	38.8	19.9 ^a	30.1 ^b	12.8 ^b	42.8 ^b	14.3 ^b	3.3	10,000	320	1.5	[71]
1.0wt%K-10wt%Fe/ZrO ₂	42.0	15.0 ^a	20.0 ^b	8.2 ^b	46.0 ^b	26.8 ^b	3.8	1200	340	2.0	[44]
Fe-Co/2.5K-Al ₂ O ₃	34.7	16.0 ^a	25 ^b	6.2 ^b	46.7 ^b	22.0 ^b	7.6	9000	340	2.0	[72]
Fe-Co/K-Al ₂ O ₃	37.2	28.9 ^b	13.5 ^b	4.2 ^b	30.2 ^b	23.2 ^b	7.3	9000 ^c	320	2.0	[38]
FeCo/NC-600	37.0	1.1 ^a	44.5 ^a	20.8 ^a	27.1 ^a	1.6 ^a	1.3	6420	320	2.0	[73]
Na-CoFe ₂ O ₄ /CNT	34.0	-	15 ^b	6 ^b	39 ^b	40 ^b	6.5	3600	340	1.0	[74]
ZnCo _{0.5} Fe _{1.5} O ₄	49.6	5.8 ^a	18.9 ^b	6.2 ^b	36.1 ^b	38.7 ^b	5.8	4800	320	2.5	[75]
35Fe-7Zr-1Ce-K	57.3	3.1 ^a	20.6 ^b	7.9 ^b	55.6 ^b	15.9 ^b	7.1	1000	320	2.0	[76]

Table 1. Cont.

Catalysts	CO ₂ Con. (%)	CO Sel. (%)	Selectivity of Hydrocarbons				O/P	Reaction Conditions			Ref.
			CH ₄	C ₂ ⁰ -C ₄ ⁰	C ₂ ⁼ -C ₄ ⁼	C ₅ ⁺		GHSV (mLg ⁻¹ h ⁻¹)	Temp. (°C)	P (Mpa)	
Fe-Cu(0.17)/K(1.0)	29.3	17.0 ^b	7.0 ^b		C ₂₊ 76.0 ^b		5.2	3600	300	1.1	[77]
CuFeO ₂	27.3	43.7 ^a	5.4 ^b	8.9 ^b	85.7 ^b	-	9.6 ^c	2400	320	1.0	[78]

^a The selectivity of product *i* was calculated by the following equation: $S_i (\%) = \frac{F_{i,out}v_i}{F_{CO_2,in} - F_{CO_2,out}} \times 100\%$, where $F_{CO_2,in}$ and $F_{CO_2,out}$ represent the inlet and outlet molar flow rates of CO₂, respectively; $F_{i,out}$ denotes the outlet molar flow rate of carbon containing product *i*; v_i refers to the carbon numbers in carbon containing product *i*. ^b The distribution of product *j* was calculated by the following equation: $D_j (\%) = \frac{F_{j,out}v_j}{\sum F_{j,out}v_j} \times 100\%$, where $F_{j,out}$ denotes the outlet molar flow rate of carbon containing product *j*; v_j refers to the carbon numbers in carbon containing product *j*. ^c Estimated based on the data in the publication.

3.1. Promoters

It was found that the incorporation of promoters could modulate the surface and interface structure of Fe-based catalysts. Various promoters, such as alkali metals [44,62–64,66,68,79–85] and non-noble metals [62,76,77,86–88] have been used to increase the specific surface area of Fe-based catalysts to modulate the CO₂ adsorption characteristics or increase the oxygen vacancies. The addition of promoters further improves the carbonation rate of Fe-based species, as well as the surface basicity or surface electron migration processes, and regulates the interaction of Fe with the supports to obtain higher CO₂ conversion and olefin selectivity.

3.1.1. Alkali Metals

Alkali metals always act as electronic promoters by donating electrons to metal atoms on the catalyst surface, and dramatically changing the catalytic activity. It was reported that Li⁺-promoted Fe-based catalysts have an inhibiting effect on the RWGS and FTS reactions [89,90]. Wang et al. [44] investigated the effects of five alkali metals on the catalytic activities of Fe/ZrO catalysts for CO₂ hydrogenation. Similar to the FTS reaction, the addition of Li⁺ suppressed both the RWGS reaction and the following CO hydrogenation reaction in CO₂ hydrogenation. The rest of the alkali metals, Na⁺, K⁺, Rb⁺ and Cs⁺, significantly decreased the selectivity to CH₄ and light paraffins, and increased it to olefins. Simultaneously, the modification by Na⁺, K⁺, or Cs⁺ also increased the conversion of CO₂. They found that the best performance for light olefin synthesis was obtained over the K⁺-modified Fe/ZrO₂ catalyst, as a result of the accelerating effect of K⁺ on the formation of the Fe₅C₂ phase. Yang et al. [91] also compared the unpromoted Fe-based catalyst with the alkali-promoted ones, as seen in Figure 3. They found that Li or Na promoters did not practically affect the activity of iron carbides to produce C₂₊ hydrocarbons, while K, Rb, or Cs promoters inhibited the activity of the catalyst. Moreover, the overall concentration of iron carbides did not depend on the kind of promoter, but the K, Rb or Cs promoters regulated the spatial distribution of active species along the catalyst bed to improve the efficiency of C₂₊ hydrocarbons production.

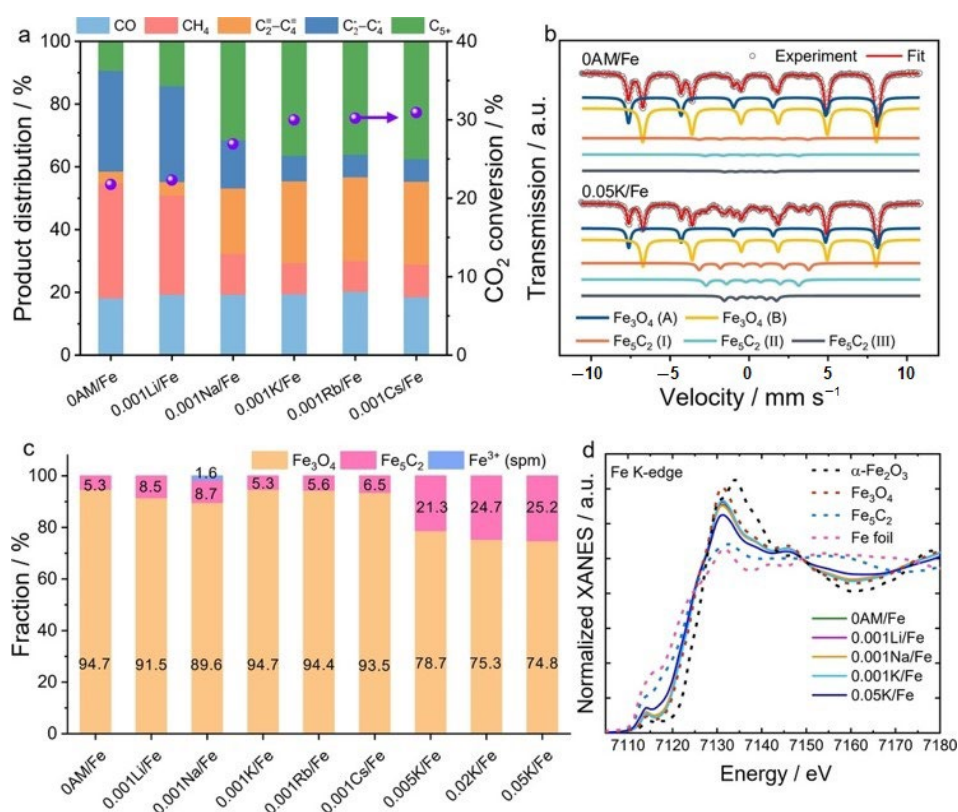


Figure 3. (a) CO₂ conversion and product distribution over 0AM/Fe and 0.001AM/Fe catalysts tested in CO₂-FTS at 15 bar and 300 °C, using a feed 3 H₂/CO₂/0.3 N₂ with a GHSV of 1160 mL g_{cat}⁻¹ h⁻¹ for 90 h. (b) Mössbauer spectra of spent 0AM/Fe and 0.05 K/Fe catalysts. (c) Composition of iron phases in spent catalysts as determined from Mössbauer spectra. (d) XANES spectra at Fe K-edge of spent 0AM/Fe, 0.001AM/Fe and 0.05 K/Fe catalysts. Reprinted with permission from ref. [91]. Copyright 2022 Wiley.

As a promising effect of K for tailoring the types of olefins in CO₂ hydrogenation, many studies have focused on K-promoted Fe-based catalysts. Wang et al. [92] studied the promotion effect of K on the carbon chain length of olefin products with single-walled carbon nanotubes (SWNTs) that support Fe catalysts in the CO₂ hydrogenation reaction. It was found that the content of K had an effect on the distribution of olefins in the products. The selectivity and productivity of light olefins (C₂=-C₄=) were highest at 7 wt.% of K, reaching 27% and 16 μmol_{CO₂} g_{Fe}⁻¹ s⁻¹, respectively; when the mass fraction of K decreased to 3%, the selectivity and productivity of heavy olefins improved to 40% and 27 μmol_{CO₂} g_{Fe}⁻¹ s⁻¹, respectively. Numpilai et al. [72] promoted Fe-Co/Al₂O₃ catalyst through the addition of K to increase the selectivity of light olefins from CO₂ hydrogenation. The positive effect of K addition was attributed to the electron donor from the K atom to the Fe species, which enhanced the bonding strength of adsorbed CO₂ and H₂ species, and retarded the hydrogenation of olefins to paraffins. Increasing the K/Fe atomic ratio from 0 to 0.5 increased the olefins/paraffins (O/P) ratio by 25.4 times. Jiang et al. [83] demonstrated that the introduction of K effectively suppressed the production of CO and CH₄, owing to its electron-donating property, promoting the adsorption and disassociation of CO, and thereby enhancing the formation of iron carbides and chain growth probability. Jiang et al. [93] investigated the surface adsorption properties of Fe-Mn samples with potassium loadings via in situ diffuse reflectance FTIR using NO, CO and CO + H₂ as probe molecules. They found that the interaction between potassium and surface iron species promoted the formation of fine metallic iron clusters, while an excess of the potassium covered the formed Fe⁰ species.

Na is also one of the most commonly used alkali metal promoters, because Na^+ in the catalyst can enhance the selectivity of light olefins by regulating the hydrogenation ability and facilitating the desorption of olefins [68]. Moreover, Na can facilitate the reduction by electron donation from Na to Fe as the oxygen vacancy formation energy is reduced by Na [20,62]. Yang et al. [84] compared the effect of sodium and potassium promoters to the zinc ferrite catalyst system on the concurrent conversion of CO and CO_2 to olefins. The Na/Fe–Zn catalyst activity for apparent CO conversion was more than twice that of the K/Fe–Zn catalyst, and it also exhibited better reactivity in terms of chain growth probability and secondary reactions. They found that the spent Na/Fe–Zn catalyst mostly consisted of Fe_5C_2 and iron oxides, whereas the amount of Fe_7C_3 in the spent K/Fe–Zn was 2.5 times higher than that in the spent Na/Fe–Zn. The density functional theory (DFT) calculations revealed that the $\chi\text{-Fe}_5\text{C}_2$ (001) surface showed weaker binding with C^* than the Fe_7C_3 (001) surface, which led to the more favorable production of the linear α -olefins on the $\chi\text{-Fe}_5\text{C}_2$ (001)-dominated surface of the Na/Fe–Zn catalyst.

Tu et al. [94] investigated in depth the role of Na in the dynamic transition of the working state of $\text{Fe}_5\text{C}_2\text{-ZnO}$ catalysts, and found that Na additive did not alter the structures of $\text{Fe}_5\text{C}_2\text{-ZnO}$, but largely improved the stability of Fe_5C_2 by preventing phase oxidation during the reaction. Furthermore, Na also modified the surface properties of the catalyst, thus facilitating the reaction of CO^* and H^* as well as C–C bond formation, as illustrated in Figure 4. Malhi et al. [69] reported that the addition of Na into Fe catalysts altered the rate dependencies on reactants, and the reaction pathways for olefins formation, which may be a result of the modification of the reducibility and surface identities of Fe catalysts by Na atoms; this changed the rate ratios of paraffins and olefins. Liang et al. [79] and Wei et al. [63] also found that the addition of Na enhanced the adsorption of CO_2 , facilitated the formation and stability of active species Fe_5C_2 , and inhibited the secondary hydrogenation of alkenes. However, Gnanamani et al. [82] revealed that the addition of alkali metals to iron oxalate decreased the bulk iron carbides formation of both the Hägg and theta carbides. The stability of iron carbides and the chain-growth probability factor for hydrocarbons and oxygenates increased with the increasing basicity of alkali added to iron for CO_2 hydrogenation.

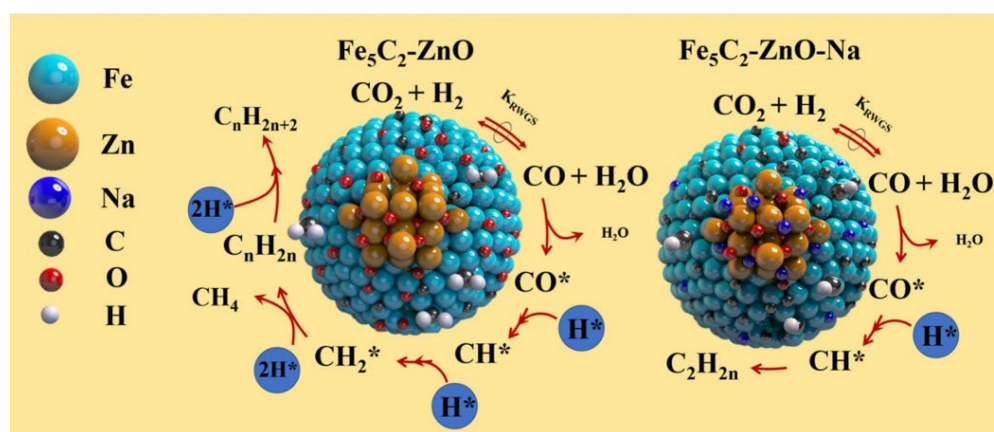


Figure 4. Plausible mechanism of Na effects on Fe_5C_2 for CO_2 hydrogenation. Reprinted with permission from ref. [94]. Copyright 2021 Elsevier.

3.1.2. Non-Noble Metals

Since the CO_2 hydrogenation reaction is a combination of the RWGS and FTS reactions, the introduction of additional FTS active sites without WGS activity is expected to accelerate CO consumption to facilitate CO_2 conversion through the FTS pathway, rather than through the WGS pathway. Jiang et al. [83] investigated the effect of introducing Co and Ru on Fe-based catalysts during CO_2 hydrogenation. The addition of Co or Ru could enhance the CO_2 conversion, only by promoting the FTS reaction rate of the CO intermediate without catalyzing the conversion of CO into CO_2 . It was found that the intimate contact between

Fe and Co sites favored a higher selectivity to C_{2+} hydrocarbons, due to the easy spillover of the CO intermediate from Fe_3O_4 to Co sites; meanwhile, the increasing distance led to a higher selectivity to CH_4 because of the lower CO concentration over Co sites. Xu et al. [75] prepared ternary $ZnCo_xFe_{2-x}O_4$ spinel nanoparticles and used them in CO_2 hydrogenation, which exhibited outstanding performance toward CO_2 hydrogenation to produce light olefins; there was a 36.1% selectivity toward $C_2=C_4$ products at a 49.6% conversion, and an unprecedentedly high iron time yield (FTY) for CO_2 conversion to light olefins ($\sim 29.1 \mu mol_{CO_2} \cdot g_{Fe}^{-1} \cdot s^{-1}$) at the gaseous hourly space velocity of $24,000 mL \cdot g_{cat}^{-1} \cdot h^{-1}$. Witton et al. [95] studied the CO_2 hydrogenation to light olefins over Fe–Co–Zn/K– Al_2O_3 catalysts with different Zn-loading contents (0–1.74 wt%). The 0.58 wt% Zn-promoted Fe–Co/K– Al_2O_3 catalyst showed superior activity for light olefins yield (19.9%) under the optimum operating conditions of $340^\circ C$, 25 bar, $9000 mL \cdot g_{cat}^{-1} \cdot h^{-1}$ and H_2 to CO_2 ratio = 4; this was due to the improvement in dispersion and the reducibility of iron oxides, and also due to an increase in active sites.

Mn is also an effective promoter to decrease methane selectivity and to increase C_2 – C_4 olefins selectivity of Fe-based catalysts during CO_2 hydrogenation [16]. It was reported that Mn acted as a structural promoter to disperse and stabilize the Fe particles [66], and promoted reduction by the presence of oxygen vacancy in MnO, as the oxygen in Fe oxide can spill over to the vacancy in MnO, spontaneously [62]. Dossary et al. [65] found that the loading amount of Mn to iron catalysts exerted a strong influence on CO_2 conversion and selectivity to different products. Liu et al. [62] suggested that to improve the selectivity of olefins, the chain growth of the alkyl-metal intermediates should be suppressed, and the short alkyl-metal intermediates should be terminated via β -H abstraction to form light olefins rather than paraffins. They found that the spatial hindrance of Mn suppressed chain growth to increase the amount of surface short alkyl-metal intermediates; furthermore, the electron transfer from Na to Fe atoms and subsequent backdonation to C^* in C-metal bonds favored the β -H abstraction of these short alkyl-metal intermediates to form light olefins. However, Xu et al. [66] demonstrated that close Fe–Mn contact could result in negative effects for both the intrinsic RWGS reaction rates and the olefin selectivity in CO_2 hydrogenation. The reason for this result was because the active phase of the catalyst transformed from the RWGS-active FeO phase to the FTS-active Fe_5C_2 phase with the assistance of Mn, whereas the steric hindrance of the Mn moiety to the FTS steps on the Fe_5C_2 sites suppressed the formation of olefins.

ZnO and Cu metals are usually used as structural promoters to adjust the Fe particle size and the exposure of active Fe metal surface. Choi et al. [20] studied a $ZnFe_2O_4$ -derived catalyst that contained well-dispersed iron particles with Zn, which served as a structural promoter to improve the selectivity of liquid-fuel to 58%, and obtained a high olefin-to-paraffin ratio of 11 in CO_2 hydrogenation. Hwang et al. [96] found that Cu could incorporate into the Fe bulk lattice in the presence of K, and that the Fe–Cu–K catalyst exhibited a C_{5+} yield of 18.1%, which was 1.4 and 7.8 times that of the FeK (12.8%) and Fe–Cu (2.3%) catalysts. Chaipraditgul et al. [97] investigated the effect of adding transition metals to Fe/K– Al_2O_3 on its catalytic activity in the reaction of CO_2 hydrogenation to olefins. It was found that Cu and Zn could significantly increase the amount of weakly adsorbed H atoms, thus improving the conversion of CO_2 as well as the selectivity of long-chain alkanes. The addition of Co also improved the conversion of CO_2 , but provided higher yields of light olefins. On the other hand, Mn and V inhibited CO hydrogenation, and consequently made the conversion of CO_2 low to some extent, but Mn reduced the weak adsorption of H atoms, and thus inhibited secondary hydrogenation of olefins to obtain a higher O/P (olefins/paraffins) value of 7.4.

3.2. Bimetallic Catalysts

Another strategy to increase CO_2 conversion and olefin yields is to introduce a secondary metal, such as Mn, Co, Cu, or Zn, to increase the reducibility and number of active sites through the high dispersion of active metals.

Similar to Fe-based catalysts, Co-based catalysts also have been developed for industrial uses in FTS. Nevertheless, in CO₂ hydrogenation at a relatively high temperature, the dominant product with Co catalysts is methane rather than C₂₊ olefins [98,99]. When the two metals are associated, the properties of the catalyst and the performance in CO₂ hydrogenation are more likely due to the formation of an iron–cobalt alloy than the simple sum of their respective properties [100]. Satthawong et al. [57,58] discovered a strong bimetallic promotion of C₂₊ hydrocarbons formation from CO₂ hydrogenation on Fe–Co catalysts by combining Fe and a small amount of Co on an alumina support. Inspired by previous research, Gnanamani et al. [35] investigated unsupported Co–Fe bimetallic catalysts in CO₂ hydrogenation, which displayed high performance at a temperature range of 200–270 °C, and at a pressure of 0.92 MPa. An increase in d spacing for the (111) plane of the metal oxalates precursor suggested that there was an incorporation of Fe into the cobalt lattice to form a Co–Fe bimetallic oxalate. After pretreatment in CO, the Co–Fe samples were composed of CoO, CoFe alloy, FeC_x, Co₂C, metallic Co and Fe, and the characterization results also showed the possibility of a presence of cobalt in the iron carbides (Figure 5a). In a subsequent study, the bimetallic alloy carbide was confirmed by Kim et al. [74], who reported that monodisperse nanoparticles of Na-promoted the CoFe₂O₄ catalysts being supported on carbon nanotubes for the preparation of C₂–C₄ olefin products by CO₂ hydrogenation (Figure 5b). In comparison with the conventional Fe₅C₂ active site of pure iron catalysts and the Co₂C active site of pure cobalt catalysts, the unique bimetallic alloy carbide (Fe_{1-x}Co_x)₅C₂ led to higher CO₂ conversion (~34%) and better selectivity toward light olefins (~39%) at 10 bar and 613 K, with an H₂/CO₂ ratio of 3:1.

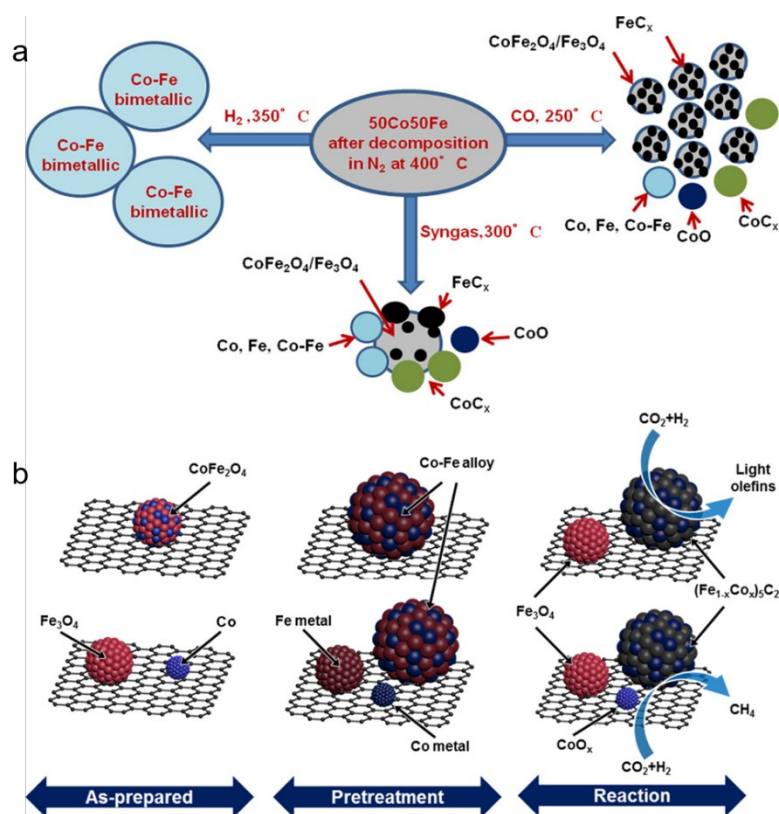


Figure 5. (a) Structures of Co–Fe bimetallic catalysts pretreated in different conditions. Reprinted with permission from ref. [35]. Copyright 2016 American Chemical Society. (b) The phase transformations of as-prepared spinel CoFe₂O₄ NPs (top row) or (Fe₃O₄ + Co) NPs (bottom row) on CNT supports during pre-reduction and reaction steps. Reprinted with permission from ref. [74]. Copyright 2020 American Chemical Society.

According to previous studies, FeO_x-MnO_x bimetallic catalysts have been proven to have excellent performance in the Fischer-Tropsch-to-olefin (FTO) process. Even a small amount of MnO_x can improve the dispersion of FeO_x and the carburization of Fe [88,101]. Kinetic studies further demonstrated the effect of MnO_x on promoting CO dissociation and monomer formation, reducing the effective sites of H₂ dissociation, olefin reabsorption and secondary hydrogenation [102], which promoted the generation of low-carbon olefins. Unlike CO hydrogenation, Kuei et al. [103] concluded that manganese showed little promotion effect on the selectivity of olefinic hydrocarbons in CO₂ hydrogenation. Generally, manganese decreased CO dissociation ability and the carbon content on catalysts, creating the proper oxide-carbide surface structure to produce olefins in CO hydrogenation. However, in CO₂ hydrogenation, this oxide/carbide surface structure may be destroyed by severe oxidation, and active carbon was unstable in an atmosphere with high water content.

Cu has high activity in both the WGS and RWGS reactions, and did not lead to the methanation of CO₂ [19]. Therefore, Fe-Cu bimetallic catalyst has attracted extensive attention in the field of CO₂ hydrogenation to olefin. Compared with monometallic Fe, the addition of Cu to Fe can successfully suppress undesired CH₄ formation, while enhancing CO and C₂₊ hydrocarbon formation [77]. Structural characterization revealed the generation of Cu-Fe alloy species, and the incorporation of Cu into the Fe bulk lattice in the presence of alkali metals [96]. Based on structural and electronic characterizations, Li et al. [78] demonstrated the reconstruction of CuFeO₂ after the activation procedure. The Cu⁺ in the CuFeO₂ lattice collapsed and aggregated to form a pure Cu phase with a partially oxidized surface. Meanwhile, Fe³⁺ in the CuFeO₂ lattice underwent partial reduction and carbonization to form Fe₃O₄, χ -Fe₅C₂ and Fe₃C. These species were in close contact with each other, forming multiple interfacial sites, such as an interface between Cu and χ -Fe₅C₂. Generally, interfacial sites between copper and iron carbides were regarded as the active center for CO insertion. As shown in Figure 6a and 6b, the DFT calculation proved that the Cu- χ -Fe₅C₂ interface significantly promoted CO insertion, relative to iron alone. Nie et al. [104,105] performed density functional theory calculations to investigate the adsorption, activation, initial hydrogenation and mechanism for CO₂ hydrogenation to C₁ and C₂ hydrocarbons over Cu-Fe bimetallic catalysts. It was found that CO₂ adsorption strength decreased monotonically as surface Cu coverage increased. On the monometallic Fe(100) surface, the favorable CH* species for production of CH₄ and C₂H₄ was formed through a path of CO₂* → CO* → HCO* → HCOH* → CH*. On the bimetallic Cu-Fe(100) surface, the preferred path for CH* formation went through CO₂* → HCOO* → HCOOH* → HCO* → HCOH* → CH* (Figure 6c). Once CH* was produced, it was more selective to CH₄ than C₂H₄ on the Fe(100) surface, since the energy barrier for C-C coupling of two CH* species was 0.3 eV higher than that for CH* to CH₄. However, on the Cu-Fe (100) surface, the barrier of CH₂ species hydrogenation was higher than that of the CH* +CH* coupling; thus, it became more favorable to produce C₂H₄ rather than CH₄.

Zn has been proven to be an effective structure promoter to disperse the active iron phases generated during the CO₂ hydrogenation reaction. Therefore, Fe-Zn bimetallic catalysts have also been investigated for enhancing olefin yields in CO₂ hydrogenation. Tu et al. [94] prepared ZnFe₂O₄ precursors, and obtained Fe₅C₂-ZnO bimetallic catalysts by CO reduction. In situ XRD detected the phase transformation of ZnFe₂O₄ to a mixture of FeO and ZnO, and then to a mixture of Fe₅C₂ and ZnO. Zhang et al. [67,106] used in situ XPS characterization to investigate the interactions of Fe-Zn bimetallic catalysts during CO₂ hydrogenation to linear α -olefins, and found that the chemical state of ZnO_x was between 0 and +2 (Zn^{δ+}), which demonstrated the electron donating interaction of Zn to Fe. They also found that adding Zn changed the balanced ratios of FeC_x/FeO_x during the reaction by preventing the oxidation of FeC_x from H₂O and CO₂, thus promoting C-C coupling and olefins synthesis over FeC_x species. An Fe₂Zn₁ catalyst showed a C₂-C₇ olefins selectivity of 57.8% in the gas phase, and a C₄-C₂₀ olefins selectivity of 60.7% with an 89.3% LAOs/olefins ratio, which was 2.4 times that of Fe₂O₃. Zhang et al. [68] proposed the reaction mechanism of CO₂ hydrogenation to olefins over Na-Zn-Fe catalysts, as shown in

Figure 7. They suggested that the CO_2 and H_2 molecules were first activated on the ZnO surface to form CO_2^* and H_2^* , followed by the hydrogenation of CO_2^* to produce CO^* and OH^* ; then, OH^* produced H_2O by combining with H^* . CO^* species near the interface diffused to the adjacent $\nu\text{-Fe}_5\text{C}_2$ surface, where hydrogenation and C–C coupling reactions occurred, followed by the formation of olefins by dehydrogenation.

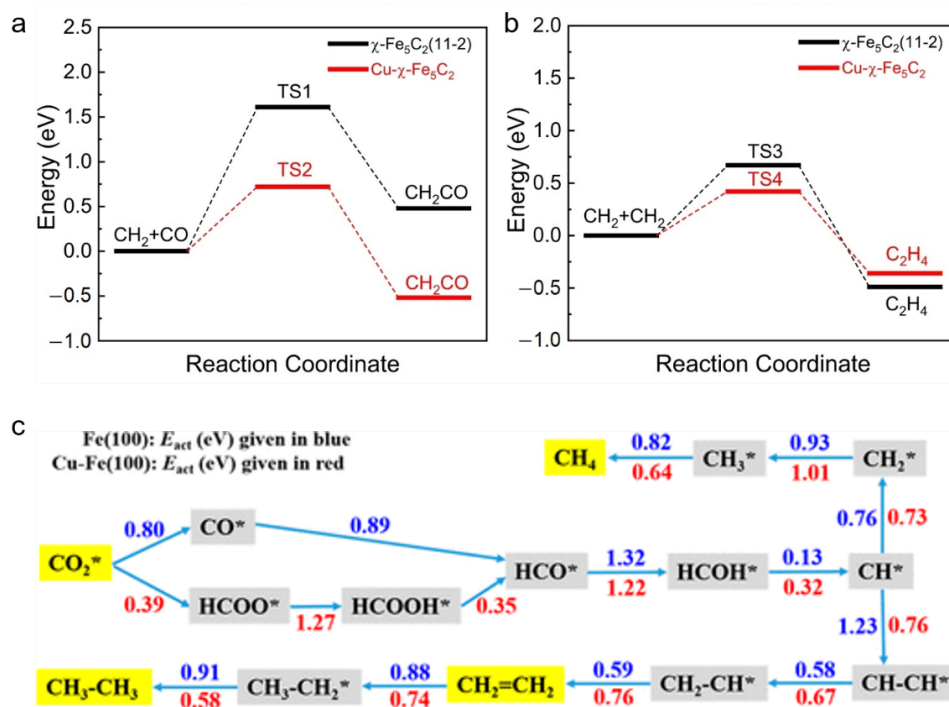


Figure 6. (a) Comparison of energy barriers of $\text{CH}_2 + \text{CO}$ over $\text{Cu-}\chi\text{-Fe}_5\text{C}_2$ and $\chi\text{-Fe}_5\text{C}_2(11-2)$ facets; (b) comparison of energy barriers of $\text{CH}_2 + \text{CH}_2$ over $\text{Cu-}\chi\text{-Fe}_5\text{C}_2$ and $\chi\text{-Fe}_5\text{C}_2(11-2)$ facets. Reprinted with permission from ref. [78]. Copyright 2022 Springer. (c) Reaction pathways for production of CH_4 , C_2H_4 and C_2H_6 from CO_2 on $\text{Fe}(100)$ and the $\text{Cu-Fe}(100)$ surface at $4/9$ ML coverage. Kinetic barrier for each elementary step is given in eV. Reprinted with permission from ref. [105]. Copyright 2017 American Chemical Society.

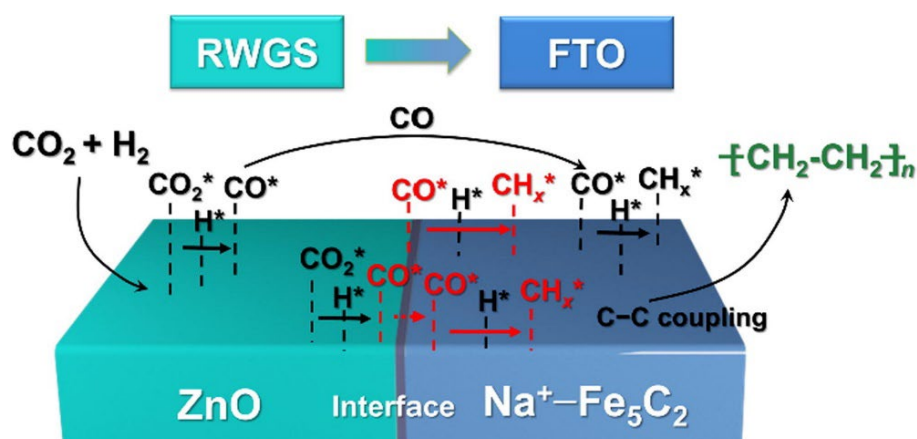


Figure 7. Reaction mechanism for CO_2 hydrogenation to olefins over the Na-Zn-Fe catalyst. Reprinted with permission from ref. [68]. Copyright 2021 Elsevier.

3.3. Supports

Using metal-support interactions to modify heterogeneous metal catalysts is an efficient way to improve the catalytic activity, and to control product selectivity during the heterogeneous catalytic reaction process. Electron transfer between metal and support [107],

support-induced recombination of metal particles, and the formation of specific interfaces between metals and supports, all contributed to the occurrence of strong metal-support interactions (SMSI) [108], which had a positive effect on the performance of catalysts [109].

3.3.1. Metal Oxides

Metal oxide-supported catalysts generally have strong metal-support interactions, as the oxide covers the metal particles during the reduction process [110]. Furthermore, when the bond between the oxide and the metal particles is strong, the metal particles become well dispersed on the oxide support [111]. Wang et al. [44] investigated the effect of supports on the catalytic performances of K⁺-modified Fe catalysts. The results showed that SiO₂ was unsuitable for CO₂ hydrogenation to hydrocarbons because both the conversion of CO₂ and the selectivity to hydrocarbons decreased over SiO₂-supported Fe-based catalysts. K⁺-modified Fe catalysts loaded onto other typical metal oxide supports, such as Al₂O₃, TiO₂, and ZrO₂, provided much better performances for the formation of light olefins. The promotion of catalytic activity by SiO₂ and Al₂O₃ was further investigated by Pandey et al. [112], who found that the SiO₂-supported Ni–Fe catalysts showed lower enhancements of conversion and yield than those observed for the Al₂O₃-supported catalysts. For the SiO₂-supported Ni–Fe catalysts, the enhancements appeared to be due to the additional metal sites formed. Moreover, from the DRIFT results, for the Al₂O₃-supported Fe–Ni catalyst, the adsorption of carbonate by the unreduced Fe₃O₄ species was a reason for the enhancements in catalytic activity. Ding et al. [113] found that the surface -OH of the ZrO₂ support had better CO₂ affinity compared to the Al₂O₃ support, and also possessed a higher surface oxygen vacancy density, all of which resulted in better catalytic activity of the catalysts. Huang et al. [71] studied the dynamic evolution of active Fe species during CO₂ hydrogenation over two kinds of zirconia (m-ZrO₂ and t-ZrO₂)-supported iron catalysts. Catalysts of 15%Fe-K/m-ZrO₂ presented a remarkable CO₂ conversion (38.8%), and a high selectivity to light olefins (42.8%). More oxygen vacancies on the surface of m-ZrO₂ and the electron-donating ability of iron elements boosted the charge transfer between Fe and the ZrO₂ support, forming a more active Fe species.

3.3.2. Carbon Materials

Chernyak et al. [114] studied CO₂ hydrogenation to hydrocarbons over spark plasma sintered Fe/CNT catalysts, which showed high activities of 5.4–12.2 mol_{CO₂} g_{Fe}^{−1} s^{−1} and promising C₂₊ selectivity of ~40–50 mol. % at low H₂:CO₂ ratios of 1 and 2, without pre-reduction. In contrast to oxide, the carbon support prevented the formation of inactive irreducible complex oxides, and promoted catalyst activation. Meanwhile, the stability of the sintered catalysts against particle migration was attributed to the framework structure of densely packed CNTs that hindered the mobility of iron-containing particles. Chew et al. [42] investigated the effects of CNT and SiO₂ as supports on the catalytic activity of Fe-based catalysts during the CO₂ hydrogenation reaction. In comparison, the iron oxide nanoparticles on SiO₂ were more difficult to reduce than on the CNT support, indicating that the interaction between iron oxide and silica was substantially stronger than that with CNTs. The strong iron–silica interaction prevented the complete reduction and carbonization of the Fe/SiO₂ catalyst, which primarily caused lower activity and high CO selectivity in CO₂ hydrogenation. The CNT-supported Fe catalysts, on the contrary, were more active and selective to light olefins in the range from C₂ to C₅. Hwang et al. [45] synthesized well-defined mesoporous carbon (MPC) as a support for Fe catalyst, which exhibited excellent catalytic activity and selectivity towards long-chain hydrocarbons (C₅₊). The mesoporous structure of MPC provided the benefits of fast mass transfer of hydrocarbon molecules, and weak metal-support interaction of MPC and Fe metal promoted the formation of Fe₇C₃ during the reaction, which generally enhanced the CO₂ conversion and C₅₊ hydrocarbon selectivity.

Metal–organic framework materials (MOFs), which consist of inorganic metal ions and organic ligands, have also been used as sacrificial templates or precursors to form

different porosities and compositions of porous carbon supports by altering the pyrolysis temperature and the components of the initial MOFs [115,116]. Dong et al. [73] prepared a carbon-encapsulated Fe–Co bimetallic catalyst using ZIF-67 as precursor support, in order to convert CO₂ to light olefins. The NC layer formed during the pyrolyzation of ZIF-67 could well embed and disperse the metal nanoparticles, which effectively promoted the reduction and carburization of the metal during the reaction. With an increase in pyrolysis temperature, the metal carburization in the reaction process became more accessible, leading to more active components of Fe₅C₂ and Co₂C. The highest selectivity of light olefins (C₂=–C₄=) of 27% was achieved using an FeCo/NC-600 catalyst, coupled with a CO₂ conversion of 37%. Similarly, Liu et al. [117,118] used ZIF-8 as a template to synthesize carbon encapsulated Fe-based catalysts, which exhibited enhanced catalytic activity toward olefins. In addition to using a MOF as a template, the corresponding catalyst could also be obtained through direct pyrolysis or carbonization of Fe-containing MOF materials, which also achieved high performance towards olefin formation [31,119]. The carbonates generated from the decarboxylation of the MOFs fully covered the particle surfaces, which could decompose to CO₂ and lead to an active surface that was rich with dangling bonds for catalytic turnover [120].

3.3.3. Zeolites

For the conventional Fe-based catalysts, hydrocarbon products generally follow the Anderson–Schulz–Flory (ASF) distribution, which is mainly composed of low-carbon linear-olefins and linear-paraffins. Considering the unique framework topology of zeolite components, they are favorable candidates for precise control of product selectivity in the oligomerization/ aromatization/ isomerization of hydrocarbons. Different types of zeolites, such as HZSM-5, HMCM-22, HBeta and HY, demonstrated unusual characteristics in the skeletal isomerization reactions of hydrocarbons [70,121–123]. Therefore, the combination of Fe-based catalysts with zeolite into a multifunctional catalyst can shift product distribution towards gasoline-range hydrocarbons and aromatics.

Wei et al. [47,70] prepared highly efficient multifunctional Na-Fe₃O₄/HMCM-22 and Na-Fe₃O₄/HZSM-5 nanocomposite catalysts to directly convert CO₂ into isoparaffins and higher hydrocarbons, respectively. Due to its unique pore structure and appropriate Brønsted acid properties, HMCM-22 effectively suppressed aromatization, while promoting isomerization to achieve a selectivity of 82% for C₄₊ hydrocarbons, of which isoparaffins accounted for 74%. The multiple active sites (Fe₃O₄, Fe₅C₂ and acid sites) in the Na-Fe₃O₄/HZSM-5 catalyst enabled a tandem reaction pathway, including the initial reduction of CO₂ to CO over the Fe₃O₄ sites, the subsequent hydrogenation of CO to olefins over the Fe₅C₂ sites, and hydrocarbon isomerization over the Brønsted acid sites in H-ZSM-5; this lead to extremely high performance in CO₂ hydrogenation with a C₅–C₁₁ hydrocarbons products selectivity of 78%, and CH₄ of only 4% at a CO₂ conversion of 22% under industrially relevant conditions. More importantly, it exhibited remarkable stability during more than 1000 h on stream, with the C₅₊ selectivity steadily maintained at 67 ± 2%.

3.3.4. Perovskite-Type Oxides

Perovskite structures are adopted by many oxides that have the chemical formula ABO₃ (perovskite-type oxides, PTOs), where A and B are two positively charged ions (i.e., cations) with very different sizes [124]. Moreover, the A and B sites can be possibly substituted by other cations, resulting in a general formula of A_{1-y}A'_yBO₃, AB_{1-x}B'_xO₃ or A_{1-y}A'_yB_{1-x}B'_xO₃ [125,126]. The unique crystal structure of PTOs can restrict the metal ions to A and B sites in specific crystals, thus providing a better dispersion of the related metal ions [127]. In addition, the metal valence state as well as the redox properties and interface structures of PTOs can be adjusted by elemental doping, or by partial substitution of the A and/or B sites, to provide controlled selectivity for the target products [128]. According to previous studies, perovskite-type catalysts have shown high catalytic activity in FTS [129–131] and RWGS reactions [132,133]. Therefore, as a potential material, Fe-doped

perovskite catalysts have also been investigated for CO₂ hydrogenation to hydrocarbons. Utsis et al. [134] investigated the effects of oxide precursors with different compositions and structures on the reactive sites of hydrogenating CO₂ on Fe-based catalysts. The results showed that solid crystalline matrix containing Fe ions with different valence states and environments strongly affected the reaction rates of the RWGS and FTS steps during CO₂ hydrogenation. The obtained ratio of $r_{\text{FTS}}/r_{\text{RWGS}}$ for the LaFe–perovskite precursor was 0.15, which indicated that there was an imbalance between the RWGS and FTS steps, and the C₅₊ hydrocarbons productivity was directly limited by the rate of the FTS step. Hou et al. [135] reported on an Sr_{1-x}K_xFeO₃ perovskite-derived catalyst with highly dispersed active sites and enhanced RWGS reaction activity, which obtained high CO₂ conversion (30.82%) and light carbon olefin selectivity (29.61%) during CO₂ hydrogenation. The K-substituted SKF_x chalcogenide catalysts were found to promote the generation of active phases (Fe₃O₄ for RWGS, Fe₅C₂ for FTS), and the catalytic performance of Fe₃O₄, the redox effect of Sr₂Fe₂O₅ on CO₂ cracking, and the formation of SrCO₃ carbonate, are responsible for the enhanced activity of the RWGS reaction. In addition, the reversible reaction between Sr₂Fe₂O₅ and CO₂ ($\text{Sr}_2\text{Fe}_2\text{O}_5 + 2\text{CO}_2 = 2\text{SrCO}_3 + \text{Fe}_2\text{O}_3$) ensured the structural stability and high dispersion of the active phase. Although the unique properties of perovskite provide many innovative ideas for catalysts construction, there are relatively few reports on the use of perovskite-derived iron catalysts for CO₂ hydrogenation to hydrocarbons. There are still many topics worthy of research in this field.

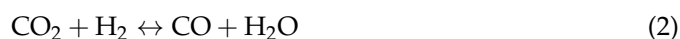
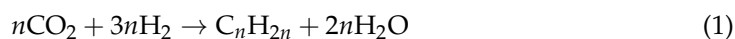
3.4. Particle Size

The size of metal particles has significant effects on their electronic and geometric effects; these changes can sometimes have unexpected effects on the catalytic activity of the catalyst. Kwak et al. [136] reported that the activity of atomically dispersed supported metals differed greatly from those of 3D metal particles in CO₂ reduction. Xie et al. [137] investigated the CO₂ hydrogenation catalytic activity of Al₂O₃-supported Fe catalysts with different pore sizes, and found that the particle size of Fe₂O₃ increased as the Al₂O₃ pore size increased, and the larger particle size facilitated the growth of C–C bonds. They found that only the appropriate Fe₂O₃ particle size (5–8 nm) was most favorable for CO₂ conversion and C₅⁺ product generation. Wu et al. [138] reported that the large difference in Ni particle size strongly affected the kinetic parameters of CO₂ hydrogenation, the formation pathways of CO and CH₄, and the reaction selectivity. Iablokov et al. [139] found that for all Co nanoparticle sizes, the TOF of CO₂ hydrogenation was found to be significantly higher on the larger nanoparticles, while the product distribution was similar. As for the CO₂ hydrogenation reaction over Fe-based catalysts, it was more difficult to study the size effect due to the complexity of the reaction pathway and products formation. Hong et al. [140] investigated the deactivation of a co-precipitated Fe–Cu–K–Al catalyst in CO₂ hydrogenation to hydrocarbons. It could be concluded that the deactivation of the Fe–Cu–K–Al catalyst was mainly caused by the growth in crystallite size and the component separation, which led to a decrease in the promoting effects of Cu and K. Zhu et al. [141] studied Fe-based catalysts with a particle size range of 2.5–12.9 nm in CO₂ hydrogenation to hydrocarbons. The overall selectivity of C₂₊ hydrocarbons increased with increasing particle size, while that of CO decreased. They found that large particles were more favorable for both the primary (RWGS and methanation) and the secondary (FTS) processes, over which the HCOO* species could be formed more easily to promote further hydrogenation to CH₄ as a primary product; moreover, large particles performed with a higher chain-growth probability. Numpilai et al. [38] found that the calcination temperature had significant impacts on metal oxides crystallite size, which affected CO₂ conversion, product selectivity, as well as the yield of olefins. They synthesized a series of Fe–Co/K–Al₂O₃ catalysts calcined at a temperatures range of 400–800 °C. With an increase in calcination temperature, a growth of metal oxides particles and a lower degree of reduction of iron oxide species were obtained. The highest CO₂ conversion (49%), hydrocarbons selectivity (90%) and olefins yield (18.1%) were achieved with Fe–Co/K–Al₂O₃

calcined at 400 °C, due to the combination of small metal oxides particles and easier reducibility of iron oxide species.

4. Active Site and Reaction Mechanism

The reaction mechanism of the CO₂ hydrogenation reaction has been controversial, due to the complexity of its intermediate species. It is generally believed that there are two pathways for the hydrogenation of CO₂ to hydrocarbons. One path is the direct hydrogenation of CO₂ to hydrocarbons (Equation (1)), and the other is the RWGS–FTS pathway, in which CO₂ is first converted to CO via the RWGS reaction (Equation (2)), and then converted to hydrocarbons via the FTS pathway of CO hydrogenation (Equation (3)). Zhu et al. [141] investigated the relationship between product selectivity and reactant conversion in the CO₂ hydrogenation reaction. It was found that CO and CH₄ selectivity were non-zero, and that C₂₊ selectivity was close to zero at a CO₂ conversion of zero. Therefore, CO and CH₄ were the primary products that were directly generated by the RWGS reaction and CO₂ methanation, and the primary CO could be subsequently converted to CH₄ and C₂₊ hydrocarbons. On this basis, the researchers proposed a reaction pathway for CO₂ hydrogenation, and considered both CO₂ methanation and the RWGS reaction as the primary reactions, and then the primary CO underwent the FTS process to form CH₄ and C₂₊ hydrocarbons. As for the mechanism of the FTS process, the common views mainly involved the CO insertion mechanism [142] and the surface carbide mechanism [143,144]. With the advancements in catalyst characterization techniques, especially the operando and in situ characterizations of catalyst surfaces, the surface carbide mechanism is becoming increasingly accepted, due to the observations of an abundance of carbon rather than oxygen on the catalyst surface. Therefore, many scholars have studied the carbon species on the catalyst surface, in order to determine the nature of the active sites during the CO/CO₂ hydrogenation reaction.



For Fe-based catalysts, the starting oxide phase is usually converted to an intermediate oxide, and eventually to a metal phase when pretreated under hydrogen-rich conditions, or to a final carbide phase under a CO-rich atmosphere [145,146], as seen in Figure 8. Since the binding strength and corresponding reactivity of the reactants vary with the Fe phases, it is necessary to understand the effect of each phase component on the catalytic reaction.

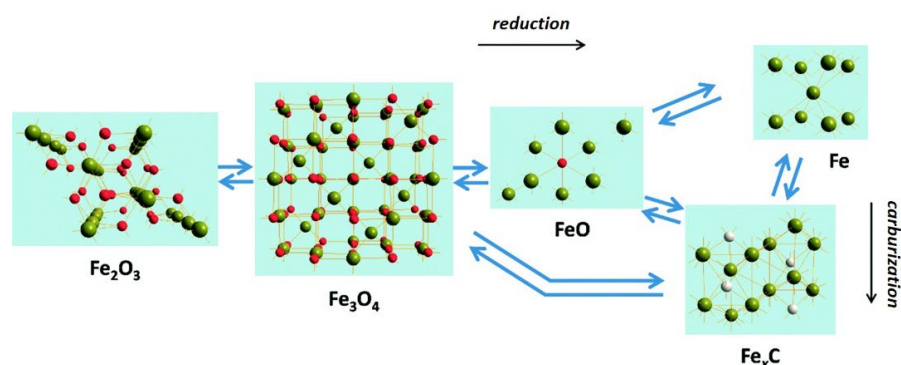


Figure 8. Schematic of the common transformations observed between different iron phases during the Fischer–Tropsch and CO₂ hydrogenation processes. Reprinted with permission from ref. [146]. Copyright 2018 Royal Society of Chemistry.

Han et al. [147] investigated the mechanism of the RWGS reaction on typical Fe-based catalyst surfaces using DFT calculations, and found that Fe₃O₄ was the active phase.

The direct dissociation mechanism of CO_2 dominated the RWGS reaction, and the OH^* removal step was the rate-determining step for most Fe-based surfaces; thus, the adsorption energy of CO_2^* and OH^* could be used as descriptors of the RWGS activity of Fe-based catalysts. Wang et al. [148] used DFT calculations to determine that HCOO^* and CH^* were key intermediates in the formation of CH_4 and C_2H_4 during CO_2 hydrogenation for hydrocarbon synthesis on the surface of $\chi\text{-Fe}_5\text{C}_2(510)$. The high surface coverage of O^* could oxidize the carbide surface, and the resulting $\text{Fe}_5\text{C}_2\text{-Fe}_2\text{O}_3$ interfacial sites facilitated the conversion of adsorbed O^* to H_2O^* , thus releasing more active sites to adsorb CH_x species, and promoting C–C coupling to produce hydrocarbons. Thus far, the common experimental observations suggest that Fe_3O_4 and iron carbides are the active phases for the RWGS and FTS reactions, respectively. Cui et al. [149] demonstrated that bare Fe_5C_2 had no activity for CO_2 conversion, and that CO_2 was first reduced to CO by H_2 via the RWGS reaction over Fe_3O_4 , followed by the subsequent CO hydrogenation to olefins via the FTS reaction on Fe_5C_2 sites. Zhang et al. [61] explored the dynamic structure–performance relationship of the iron catalyst throughout its full lifecycle in CO_2 hydrogenation to olefins. When pretreated in a CO atmosphere, the phase change process of iron in the catalyst followed $\text{Fe}_2\text{O}_3 \rightarrow \text{Fe}_3\text{O}_4 \rightarrow \text{Fe} \rightarrow \text{Fe}_5\text{C}_2$. After the reaction gas was introduced, the phase change process had two main paths, which were $\text{Fe}_5\text{C}_2 \rightarrow \text{Fe}_3\text{O}_4$ and $\text{Fe}_5\text{C}_2 \rightarrow \text{Fe}_3\text{C} \rightarrow \text{Fe}_3\text{O}_4$. The results showed that the Fe_5C_2 phase was the active phase for the generation of $\text{C}_2\text{-C}_4$ olefins. The irreversible oxidation of the iron carbides to Fe_3O_4 under CO_2 hydrogenation conditions was the main factor leading to catalyst deactivation (Figure 9).

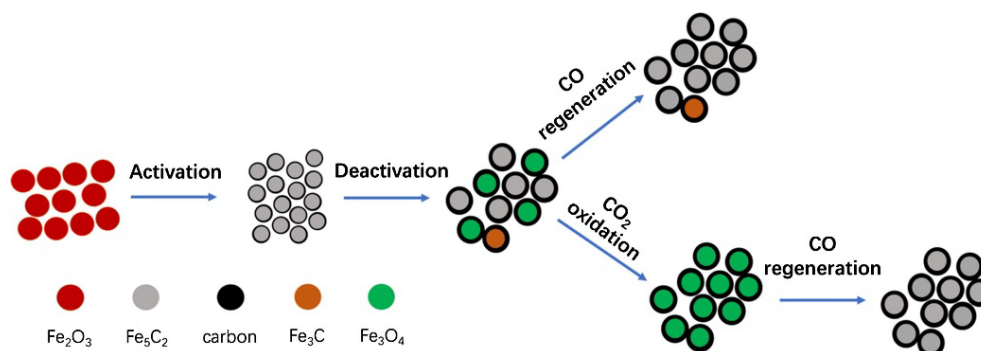


Figure 9. Structure evolution of Fe catalyst in CO_2 hydrogenation during its life cycle. Reprinted with permission from ref. [61]. Copyright 2019 Elsevier.

In fact, Fe-based catalysts have been observed to form a variety of iron carbides in the FTS reaction, such as $\epsilon\text{-Fe}_2\text{C}$, $\epsilon'\text{-Fe}_{2.2}\text{C}$, Fe_7C_3 , $\chi\text{-Fe}_5\text{C}_2$ and $\theta\text{-Fe}_3\text{C}$ [150,151]. Figure 10 shows the structures of iron carbides and their transformation pathway obtained by the Ab initio atomistic thermodynamics method, which showed that iron carbides can be transformed into each other under certain conditions [152].

It is necessary to figure out the catalytic activities of different iron carbide phases. Smit et al. [152] investigated the stability and reactivity of each iron carbide phase at different carbon chemical potentials, and found that $\chi\text{-Fe}_5\text{C}_2$ was susceptible to oxidation under FTS reaction conditions, while Fe_3C and amorphous iron carbides exhibited lower activity and selectivity. However, Mazzucco et al. [153] presented direct evidence that nanoparticles with the cementite (Fe_3C) structure were active for nanotube growth (C–C bond formation), while carbon-rich particles with the Hägg (Fe_5C_2) structure were inactive. Density functional theory calculations suggested that reduced activity may be due to lower carbon mobility and higher C–C bond formation energies on the surface of nanoparticles with a Fe_5C_2 structure. Zhang et al. [41] also found a significant difference in the catalytic activities of $\chi\text{-Fe}_5\text{C}_2$ and $\theta\text{-Fe}_3\text{C}$ generated from $\alpha\text{-Fe}_2\text{O}_3$ and $\gamma\text{-Fe}_2\text{O}_3$ in the CO_2 hydrogenation reaction. The higher selectivity of $\chi\text{-Fe}_5\text{C}_2$ over light olefins was attributed to its higher effective barrier and weaker hydrogenation ability, while the high

selectivity of C_{5+} hydrocarbons on θ - Fe_3C was mainly attributed to its strong adsorption of CO_2 , enhancing the chain growth of the adsorbed carbonaceous species (Figure 11). Yang et al. [154] synthesized different iron carbides (Fe_5C_2 , Fe_5C_2 and Fe_3C mixture, Fe_3C) by varying the carburization temperature of iron oxalate precursors between 320 and 450 °C, and tested their catalytic activity in a CO hydrogenation reaction. The results showed that both CO conversion and product selectivity were influenced by the iron carbides. The CO conversion and the selectivity of light olefins were higher when Fe_5C_2 was the dominant iron carbide. In addition, the selectivity of C_{5+} hydrocarbons in the products was higher when Fe_3C was present alone.

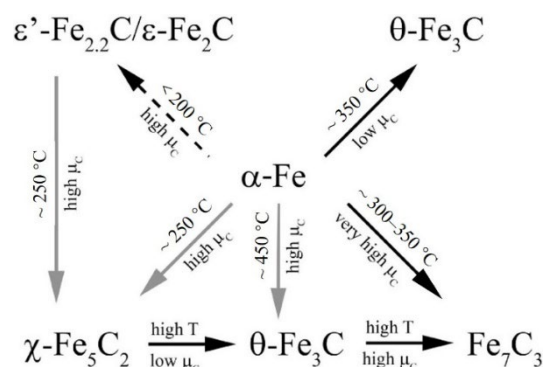


Figure 10. Qualitative interpretation of the ab initio atomistic thermodynamics study of iron carbides structures (gray arrows indicate transformations where entropic contributions to the total free energy may be significant. The dashed arrow indicates that the transformation may be kinetically inhibited). Reprinted with permission from ref. [152]. Copyright 2010 American Chemical Society.

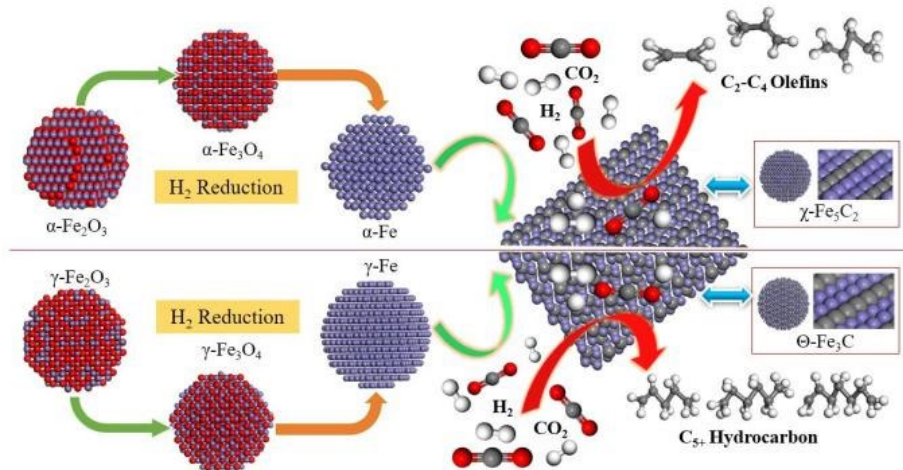


Figure 11. Scheme of the structure–performance relationship of α - Fe_2O_3 and γ - Fe_2O_3 catalysts for CO_2 hydrogenation during activation and reaction processes. Reprinted with permission from ref. [41]. Copyright 2018 John Wiley and Sons.

5. Conclusions

In the face of severe pressure for CO_2 reduction, developing approaches that utilize CO_2 resources efficiently is a challenging topic in C1 chemistry research. The direct synthesis of olefins via catalytic CO_2 hydrogenation is one of the promising ways to realize the conversion and utilization of CO_2 . Fe-based catalysts are widely used for CO_2 hydrogenation to hydrocarbons, due to their cost-effective performance and catalytic activity. However, under reaction conditions, complex and diverse phases such as iron oxide, metallic iron and iron carbide may co-exist on Fe-based catalysts as the active phases for the reactions of CO_2 activation, H_2 activation, CO hydrogenation, carbon chain growth and hydrogenation, respectively, which make the characterization of the dynamic structural

evolution of Fe-based catalysts even more challenging. In recent years, many studies have tried to tune the morphology structures, reducibility, surface basicity, and adsorption properties of Fe-based catalysts, by altering the methods and temperatures of catalyst syntheses, supports, and promoters, or introducing other elements to form Fe-based bimetallic clusters. Although these studies are devoted to improving CO₂ conversion and olefin selectivity, the catalytic consequences of the changes in structure at the surface and interface of Fe-based catalysts on the rate of CO₂ hydrogenation activation, and the distribution pattern of carbon-containing products, are still insufficient and controversial. Meanwhile, the reaction pathways and kinetics of CO₂ hydrogenation to olefins over Fe-based catalysts are still not well-established, which restrict the precise regulation of the catalysts' active center, the design of industrial catalytic reactors, and limit the scale-up of CO₂ hydrogenation to olefins.

Therefore, in addition to constructing highly active iron-based catalysts to further inhibit the generation of by-products such as CH₄ and improve the selectivity of target products, it is also necessary to combine in situ or operando characterizations and DFT calculations to deeply analyze the active sites for CO₂ activation and C=C bond formation on iron-based catalysts under realistic reaction conditions, and the resulting reaction pathways for CO₂ hydrogenation. Clarification of the structure–performance relationships of iron-based catalysts in the CO₂ hydrogenation process will facilitate the precise regulation of the active center of catalysts, and the design of industrial reactors that are suitable for scale-up of CO₂ utilization.

Author Contributions: Conceptualization: W.L. and W.T.; validation: W.L. and W.T.; formal analysis: W.L., S.C., H.S.M. and W.T.; writing—original draft preparation: W.L. and W.T.; writing—review and editing: W.L., S.C., H.S.M., X.G., Z.Z. and W.T.; supervision: W.T. and Z.Z.; funding acquisition: W.T. and Z.Z. All authors have read and agreed to the published version of the manuscript.

Funding: This research was funded by the National Natural Science Foundation of China (Project No. 22078307, 22238003, 22208314, 22278379), Natural Science Foundation of Henan Province (202300410432), the State Key Laboratory of Coal Conversion (J21-22-902), and the State Key Laboratory of High efficiency Utilization of Coal and Green Chemical Engineering (2022-K05 and 2022-K21).

Data Availability Statement: Not applicable.

Conflicts of Interest: The authors declare no conflict of interest.

References

1. IEA. *Global Energy Review: CO₂ Emissions in 2021*; IEA: Paris, France, 2022. Available online: <https://www.iea.org/reports/global-energy-review-co2-emissions-in-2021-2> (accessed on 3 October 2022).
2. Observatory, M.L. Atmospheric CO₂. Available online: <https://www.co2.earth/> (accessed on 3 October 2022).
3. Broecker, W.S. CO₂ Arithmetic. *Science* **2007**, *315*, 1371. [[CrossRef](#)] [[PubMed](#)]
4. Huang, C.H.; Tan, C.S. A Review: CO₂ Utilization. *Aerosol. Air Qual. Res.* **2014**, *14*, 480–499. [[CrossRef](#)]
5. Haszeldine, R.S. Carbon Capture and Storage: How Green Can Black Be? *Science* **2009**, *325*, 1647–1652. [[CrossRef](#)]
6. Boot-Handford, M.E.; Abanades, J.C.; Anthony, E.J.; Blunt, M.J.; Brandani, S.; Mac Dowell, N.; Fernández, J.R.; Ferrari, M.-C.; Gross, R.; Hallett, J.P.; et al. Carbon capture and storage update. *Energy Environ. Sci.* **2014**, *7*, 130–189. [[CrossRef](#)]
7. Yang, H.; Zhang, C.; Gao, P.; Wang, H.; Li, X.; Zhong, L.; Wei, W.; Sun, Y. A review of the catalytic hydrogenation of carbon dioxide into value-added hydrocarbons. *Catal. Sci. Technol.* **2017**, *7*, 4580–4598. [[CrossRef](#)]
8. Ra, E.C.; Kim, K.Y.; Kim, E.H.; Lee, H.; An, K.; Lee, J.S. Recycling Carbon Dioxide through Catalytic Hydrogenation: Recent Key Developments and Perspectives. *ACS Catal.* **2020**, *10*, 11318–11345. [[CrossRef](#)]
9. Lim, X. How to make the most of carbon dioxide. *Nature* **2015**, *526*, 628–630. [[CrossRef](#)]
10. MacDowell, N.; Florin, N.; Buchard, A.; Hallett, J.; Galindo, A.; Jackson, G.; Adjiman, C.S.; Williams, C.K.; Shah, N.; Fennell, P. An overview of CO₂ capture technologies. *Energy Environ. Sci.* **2010**, *3*, 1645–1669. [[CrossRef](#)]
11. Skrypnik, A.S.; Yang, Q.X.; Matvienko, A.A.; Bychkov, V.Y.; Tulenin, Y.P.; Lund, H.; Petrov, S.A.; Kraehnert, R.; Arinchtin, A.; Weiss, J.; et al. Understanding reaction-induced restructuring of well-defined Fe_xO_yC_z compositions and its effect on CO₂ hydrogenation. *Appl. Catal. B-Environ.* **2021**, *291*, 11. [[CrossRef](#)]
12. Dokania, A.; Ramirez, A.; Bavykina, A.; Gascon, J. Heterogeneous Catalysis for the Valorization of CO₂: Role of Bifunctional Processes in the Production of Chemicals. *ACS Energy Lett.* **2019**, *4*, 167–176. [[CrossRef](#)]

13. Prieto, G. Carbon Dioxide Hydrogenation into Higher Hydrocarbons and Oxygenates: Thermodynamic and Kinetic Bounds and Progress with Heterogeneous and Homogeneous Catalysis. *ChemSusChem* **2017**, *10*, 1056–1070. [[CrossRef](#)] [[PubMed](#)]
14. Zhou, W.; Cheng, K.; Kang, J.C.; Zhou, C.; Subramanian, V.; Zhang, Q.H.; Wang, Y. New horizon in C1 chemistry: Breaking the selectivity limitation in transformation of syngas and hydrogenation of CO₂ into hydrocarbon chemicals and fuels. *Chem. Soc. Rev.* **2019**, *48*, 3193–3228. [[CrossRef](#)] [[PubMed](#)]
15. Das, S.; Perez-Ramirez, J.; Gong, J.; Dewangan, N.; Hidajat, K.; Gates, B.C.; Kawi, S. Core-shell structured catalysts for thermocatalytic, photocatalytic, and electrocatalytic conversion of CO₂. *Chem. Soc. Rev.* **2020**, *49*, 2937–3004. [[CrossRef](#)] [[PubMed](#)]
16. Galvis, H.M.T.; de Jong, K.P. Catalysts for Production of Lower Olefins from Synthesis Gas: A Review. *ACS Catal.* **2013**, *3*, 2130–2149. [[CrossRef](#)]
17. Liang, B.; Duan, H.; Hou, B.; Su, X.; Huang, Y.; Wang, A.; Wang, X.; Zhang, T. Progress in the catalytic hydrogenation of carbon dioxide to light olefins. *Chem. Ind. Eng. Prog.* **2015**, *34*, 3746–3754.
18. Choi, Y.H.; Jang, Y.J.; Park, H.; Kim, W.Y.; Lee, Y.H.; Choi, S.H.; Lee, J.S. Carbon dioxide Fischer-Tropsch synthesis: A new path to carbon-neutral fuels. *Appl. Catal. B-Environ.* **2017**, *202*, 605–610. [[CrossRef](#)]
19. Centi, G.; Perathoner, S. Opportunities and prospects in the chemical recycling of carbon dioxide to fuels. *Catal. Today* **2009**, *148*, 191–205. [[CrossRef](#)]
20. Choi, Y.H.; Ra, E.C.; Kim, E.H.; Kim, K.Y.; Jang, Y.J.; Kang, K.N.; Choi, S.H.; Jang, J.H.; Lee, J.S. Sodium-Containing Spinel Zinc Ferrite as a Catalyst Precursor for the Selective Synthesis of Liquid Hydrocarbon Fuels. *ChemSusChem* **2017**, *10*, 4764–4770. [[CrossRef](#)]
21. Van Speybroeck, V.; De Wispelaere, K.; Van der Mynsbrugge, J.; Vandichel, M.; Hemelsoet, K.; Waroquier, M. First principle chemical kinetics in zeolites: The methanol-to-olefin process as a case study. *Chem. Soc. Rev.* **2014**, *43*, 7326–7357. [[CrossRef](#)]
22. Tian, P.; Wei, Y.; Ye, M.; Liu, Z. Methanol to Olefins (MTO): From Fundamentals to Commercialization. *ACS Catal.* **2015**, *5*, 1922–1938. [[CrossRef](#)]
23. Bjørgen, M.; Joensen, F.; Spangsbjerg Holm, M.; Olsbye, U.; Lillerud, K.-P.; Svelle, S. Methanol to gasoline over zeolite H-ZSM-5: Improved catalyst performance by treatment with NaOH. *Appl. Catal. A-Gen.* **2008**, *345*, 43–50. [[CrossRef](#)]
24. Olsbye, U.; Svelle, S.; Bjørgen, M.; Beato, P.; Janssens, T.V.W.; Joensen, F.; Bordiga, S.; Lillerud, K.P. Conversion of Methanol to Hydrocarbons: How Zeolite Cavity and Pore Size Controls Product Selectivity. *Angew. Chem. Int. Ed.* **2012**, *51*, 5810–5831. [[CrossRef](#)] [[PubMed](#)]
25. Li, Z.; Wang, J.; Qu, Y.; Liu, H.; Tang, C.; Miao, S.; Feng, Z.; An, H.; Li, C. Highly Selective Conversion of Carbon Dioxide to Lower Olefins. *ACS Catal.* **2017**, *7*, 8544–8548. [[CrossRef](#)]
26. Numpilai, T.; Cheng, C.K.; Limtrakul, J.; Witoon, T. Recent advances in light olefins production from catalytic hydrogenation of carbon dioxide. *Process Saf. Environ. Prot.* **2021**, *151*, 401–427. [[CrossRef](#)]
27. Ojelade, O.A.; Zaman, S.F. A review on CO₂ hydrogenation to lower olefins: Understanding the structure-property relationships in heterogeneous catalytic systems. *J. CO₂ Util.* **2021**, *47*, 101506. [[CrossRef](#)]
28. Sedighi, M.; Mohammadi, M. CO₂ hydrogenation to light olefins over Cu-CeO₂/SAPO-34 catalysts: Product distribution and optimization. *J. CO₂ Util.* **2020**, *35*, 236–244. [[CrossRef](#)]
29. Wang, D.; Xie, Z.; Porosoff, M.D.; Chen, J.G. Recent advances in carbon dioxide hydrogenation to produce olefins and aromatics. *Chem* **2021**, *7*, 2277–2311. [[CrossRef](#)]
30. Santos, V.P.; Wezendonk, T.A.; Jaén, J.J.D.; Dugulan, A.I.; Nasalevich, M.A.; Islam, H.-U.; Chojecki, A.; Sartipi, S.; Sun, X.; Hakeem, A.A.; et al. Metal organic framework-mediated synthesis of highly active and stable Fischer-Tropsch catalysts. *Nat. Commun.* **2015**, *6*, 6451. [[CrossRef](#)]
31. Ramirez, A.; Gevers, L.; Bavykina, A.; Ould-Chikh, S.; Gascon, J. Metal Organic Framework-Derived Iron Catalysts for the Direct Hydrogenation of CO₂ to Short Chain Olefins. *ACS Catal.* **2018**, *8*, 9174–9182. [[CrossRef](#)]
32. Hu, B.; Frueh, S.; Garces, H.F.; Zhang, L.; Aindow, M.; Brooks, C.; Kreidler, E.; Suib, S.L. Selective hydrogenation of CO₂ and CO to useful light olefins over octahedral molecular sieve manganese oxide supported iron catalysts. *Appl. Catal. B-Environ.* **2013**, *132–133*, 54–61. [[CrossRef](#)]
33. Wang, Q.; Chen, Y.; Li, Z.H. Research Progress of Catalysis for Low-Carbon Olefins Synthesis through Hydrogenation of CO₂. *J. Nanosci. Nanotechnol.* **2019**, *19*, 3162–3172. [[CrossRef](#)] [[PubMed](#)]
34. Visconti, C.G.; Lietti, L.; Tronconi, E.; Forzatti, P.; Zennaro, R.; Finocchio, E. Fischer-Tropsch synthesis on a Co/Al₂O₃ catalyst with CO₂ containing syngas. *Appl. Catal. A-Gen.* **2009**, *355*, 61–68. [[CrossRef](#)]
35. Gnanamani, M.K.; Jacobs, G.; Hamdeh, H.H.; Shafer, W.D.; Liu, F.; Hopps, S.D.; Thomas, G.A.; Davis, B.H. Hydrogenation of Carbon Dioxide over Co-Fe Bimetallic Catalysts. *ACS Catal.* **2016**, *6*, 913–927. [[CrossRef](#)]
36. Abelló, S.; Montané, D. Exploring iron-based multifunctional catalysts for Fischer-Tropsch synthesis: A review. *ChemSusChem* **2011**, *4*, 1538–1556. [[CrossRef](#)]
37. Wang, X.; Zhang, J.; Chen, J.; Ma, Q.; Fan, S.; Zhao, T.-s. Effect of preparation methods on the structure and catalytic performance of Fe-Zn/K catalysts for CO₂ hydrogenation to light olefins. *Chin. J. Chem. Eng.* **2018**, *26*, 761–767. [[CrossRef](#)]
38. Numpilai, T.; Witoon, T.; Chanlek, N.; Limphirat, W.; Bonura, G.; Chareonpanich, M.; Limtrakul, J. Structure-activity relationships of Fe-Co/K-Al₂O₃ catalysts calcined at different temperatures for CO₂ hydrogenation to light olefins. *Appl. Catal. A-Gen.* **2017**, *547*, 219–229. [[CrossRef](#)]

39. Herranz, T.; Rojas, S.; Perez-Alonso, F.J.; Ojeda, M.; Terreros, P.; Fierro, J.L.G. Genesis of iron carbides and their role in the synthesis of hydrocarbons from synthesis gas. *J. Catal.* **2006**, *243*, 199–211. [[CrossRef](#)]
40. Sirikulbodee, P.; Ratana, T.; Sornchamni, T.; Phongaksorn, M.; Tungkamani, S. Catalytic performance of Iron-based catalyst in Fischer-Tropsch synthesis using CO₂ containing syngas. In Proceedings of the 2017 International Conference on Alternative Energy in Developing Countries and Emerging Economies, Bangkok, Thailand, 25–26 May 2017; pp. 998–1003.
41. Zhang, Y.L.; Fu, D.L.; Liu, X.L.; Zhang, Z.P.; Zhang, C.; Shi, B.F.; Xu, J.; Han, Y.F. Operando Spectroscopic Study of Dynamic Structure of Iron Oxide Catalysts during CO₂ Hydrogenation. *Chemcatchem* **2018**, *10*, 1272–1276. [[CrossRef](#)]
42. Chew, L.M.; Kangvansura, P.; Ruland, H.; Schulte, H.J.; Somsen, C.; Xia, W.; Eggeler, G.; Worayingyong, A.; Muhler, M. Effect of nitrogen doping on the reducibility, activity and selectivity of carbon nanotube-supported iron catalysts applied in CO₂ hydrogenation. *Appl. Catal. A-Gen.* **2014**, *482*, 163–170. [[CrossRef](#)]
43. Yang, Q.; Skrypnik, A.; Matvienko, A.; Lund, H.; Holena, M.; Kondratenko, E.V. Revealing property-performance relationships for efficient CO₂ hydrogenation to higher hydrocarbons over Fe-based catalysts: Statistical analysis of literature data and its experimental validation. *Appl. Catal. B-Environ.* **2021**, *282*, 119554. [[CrossRef](#)]
44. Wang, J.J.; You, Z.Y.; Zhang, Q.H.; Deng, W.P.; Wang, Y. Synthesis of lower olefins by hydrogenation of carbon dioxide over supported iron catalysts. *Catal. Today* **2013**, *215*, 186–193. [[CrossRef](#)]
45. Hwang, S.M.; Zhang, C.D.; Han, S.J.; Park, H.G.; Kim, Y.T.; Yang, S.; Jun, K.W.; Kim, S.K. Mesoporous carbon as an effective support for Fe catalyst for CO₂ hydrogenation to liquid hydrocarbons. *J. CO₂ Util.* **2020**, *37*, 65–73. [[CrossRef](#)]
46. Suppiah, D.D.; Daud, W.M.A.W.; Johan, M.R. Supported Metal Oxide Catalysts for CO₂ Fischer-Tropsch Conversion to Liquid Fuels—A Review. *Energy Fuels* **2021**, *35*, 17261–17278. [[CrossRef](#)]
47. Wei, J.; Yao, R.; Ge, Q.; Wen, Z.; Ji, X.; Fang, C.; Zhang, J.; Xu, H.; Sun, J. Catalytic Hydrogenation of CO₂ to Isoparaffins over Fe-Based Multifunctional Catalysts. *ACS Catal.* **2018**, *8*, 9958–9967. [[CrossRef](#)]
48. Albrecht, M.; Rodemerck, U.; Schneider, M.; Broering, M.; Baabe, D.; Kondratenko, E.V. Unexpectedly efficient CO₂ hydrogenation to higher hydrocarbons over non-doped Fe₂O₃. *Appl. Catal. B-Environ.* **2017**, *204*, 119–126. [[CrossRef](#)]
49. Riedel, T.; Schaub, G.; Jun, K.W.; Lee, K.W. Kinetics of CO₂ hydrogenation on a K-promoted Fe catalyst. *Ind. Eng. Chem. Res.* **2001**, *40*, 1355–1363. [[CrossRef](#)]
50. Yao, B.Z.; Ma, W.J.; Gonzalez-Cortes, S.; Xiao, T.C.; Edwards, P.P. Thermodynamic study of hydrocarbon synthesis from carbon dioxide and hydrogen. *Greenh. Gases Sci. Technol.* **2017**, *7*, 942–957. [[CrossRef](#)]
51. Liu, Y.K.; Wang, L.; Hou, D.; Wan, H.; Feng, X. Study on thermodynamics of balanceable reaction system for hydrogenation of carbon dioxide to light alkenes. *Chin. J. Catal.* **2004**, *25*, 210–218. [[CrossRef](#)]
52. Torrente-Murciano, L.; Mattia, D.; Jones, M.D.; Plucinski, P.K. Formation of hydrocarbons via CO₂ hydrogenation - A thermodynamic study. *J. CO₂ Util.* **2014**, *6*, 34–39. [[CrossRef](#)]
53. Riedel, T.; Claeys, M.; Schulz, H.; Schaub, G.; Nam, S.S.; Jun, K.W.; Choi, M.J.; Kishan, G.; Lee, K.W. Comparative study of Fischer-Tropsch synthesis with H₂/CO and H₂/CO₂ syngas using Fe- and Co-based catalysts. *Appl. Catal. Gen.* **1999**, *186*, 201–213. [[CrossRef](#)]
54. Jiao, F.; Li, J.; Pan, X.; Xiao, J.; Li, H.; Ma, H.; Wei, M.; Pan, Y.; Zhou, Z.; Li, M.; et al. Selective conversion of syngas to light olefins. *Science* **2016**, *351*, 1065–1068. [[CrossRef](#)] [[PubMed](#)]
55. Torres Galvis, H.M.; Koeken, A.C.J.; Bitter, J.H.; Davidian, T.; Ruitenbeek, M.; Dugulan, A.I.; de Jong, K.P. Effects of sodium and sulfur on catalytic performance of supported iron catalysts for the Fischer-Tropsch synthesis of lower olefins. *J. Catal.* **2013**, *303*, 22–30. [[CrossRef](#)]
56. Galvis, H.M.T.; Bitter, J.H.; Khare, C.B.; Ruitenbeek, M.; Dugulan, A.I.; Jong, K.P.d. Supported Iron Nanoparticles as Catalysts for Sustainable Production of Lower Olefins. *Science* **2012**, *335*, 835–838. [[CrossRef](#)] [[PubMed](#)]
57. Sathawong, R.; Koizumi, N.; Song, C.; Prasassarakich, P. Bimetallic Fe-Co catalysts for CO₂ hydrogenation to higher hydrocarbons. *J. CO₂ Util.* **2013**, *3-4*, 102–106. [[CrossRef](#)]
58. Sathawong, R.; Koizumi, N.; Song, C.; Prasassarakich, P. Light olefin synthesis from CO₂ hydrogenation over K-promoted Fe-Co bimetallic catalysts. *Catal. Today* **2015**, *251*, 34–40. [[CrossRef](#)]
59. Li, Y.; Li, L.; Yu, J. Applications of Zeolites in Sustainable Chemistry. *Chem* **2017**, *3*, 928–949. [[CrossRef](#)]
60. Sun, J.; Li, X.; Taguchi, A.; Abe, T.; Niu, W.; Lu, P.; Yoneyama, Y.; Tsubaki, N. Highly-Dispersed Metallic Ru Nanoparticles Sputtered on H-Beta Zeolite for Directly Converting Syngas to Middle Isoparaffins. *ACS Catal.* **2014**, *4*, 1–8. [[CrossRef](#)]
61. Zhang, Y.L.; Cao, C.X.; Zhang, C.; Zhang, Z.P.; Liu, X.L.; Yang, Z.X.; Zhu, M.H.; Meng, B.; Xu, J.; Han, Y.F. The study of structure-performance relationship of iron catalyst during a full life cycle for CO₂ hydrogenation. *J. Catal.* **2019**, *378*, 51–62. [[CrossRef](#)]
62. Liu, B.; Geng, S.; Zheng, J.; Jia, X.; Jiang, F.; Liu, X. Unravelling the New Roles of Na and Mn Promoter in CO₂ Hydrogenation over Fe₃O₄-Based Catalysts for Enhanced Selectivity to Light-Olefins. *Chemcatchem* **2018**, *10*, 4718–4732. [[CrossRef](#)]
63. Wei, C.Y.; Tu, W.F.; Jia, L.Y.; Liu, Y.Y.; Lian, H.L.; Wang, P.; Zhang, Z.Z. The evolutions of carbon and iron species modified by Na and their tuning effect on the hydrogenation of CO₂ to olefins. *Appl. Surf. Sci.* **2020**, *525*, 13. [[CrossRef](#)]
64. Wei, J.; Sun, J.; Wen, Z.; Fang, C.; Ge, Q.; Xu, H. New insights into the effect of sodium on Fe₃O₄-based nanocatalysts for CO₂ hydrogenation to light olefins. *Catal. Sci. Technol.* **2016**, *6*, 4786–4793. [[CrossRef](#)]
65. Al-Dossary, M.; Ismail, A.A.; Fierro, J.L.G.; Bouzid, H.; Al-Sayari, S.A. Effect of Mn loading onto MnFeO nanocomposites for the CO₂ hydrogenation reaction. *Appl. Catal. B-Environ.* **2015**, *165*, 651–660. [[CrossRef](#)]

66. Xu, Y.; Zhai, P.; Deng, Y.; Xie, J.; Liu, X.; Wang, S.; Ma, D. Highly Selective Olefin Production from CO₂ Hydrogenation on Iron Catalysts: A Subtle Synergy between Manganese and Sodium Additives. *Angew. Chem. Int. Ed.* **2020**, *59*, 21736–21744. [[CrossRef](#)] [[PubMed](#)]
67. Zhang, C.; Xu, M.J.; Yang, Z.X.; Zhu, M.H.; Gao, J.; Han, Y.F. Uncovering the electronic effects of zinc on the structure of Fe₅C₂-ZnO catalysts for CO₂ hydrogenation to linear alpha-olefins. *Appl. Catal. B-Environ.* **2021**, *295*, 11. [[CrossRef](#)]
68. Zhang, Z.Q.; Yin, H.R.; Yu, G.D.; He, S.; Kang, J.C.; Liu, Z.M.; Cheng, K.; Zhang, Q.H.; Wang, Y. Selective hydrogenation of CO₂ and CO into olefins over Sodium- and Zinc-Promoted iron carbide catalysts. *J. Catal.* **2021**, *395*, 350–361. [[CrossRef](#)]
69. Malhi, H.S.; Sun, C.; Zhang, Z.; Liu, Y.; Liu, W.; Ren, P.; Tu, W.; Han, Y.-F. Catalytic consequences of the decoration of sodium and zinc atoms during CO₂ hydrogenation to olefins over iron-based catalyst. *Catal. Today* **2022**, *387*, 28–37. [[CrossRef](#)]
70. Wei, J.; Ge, Q.; Yao, R.; Wen, Z.; Fang, C.; Guo, L.; Xu, H.; Sun, J. Directly converting CO₂ into a gasoline fuel. *Nat. Commun.* **2017**, *8*, 15174. [[CrossRef](#)]
71. Huang, J.; Jiang, S.; Wang, M.; Wang, X.; Gao, J.; Song, C. Dynamic Evolution of Fe and Carbon Species over Different ZrO₂ Supports during CO Prereduction and Their Effects on CO₂ Hydrogenation to Light Olefins. *ACS Sustain. Chem. Eng.* **2021**, *9*, 7891–7903. [[CrossRef](#)]
72. Numpilai, T.; Chanlek, N.; Poo-Arporn, Y.; Cheng, C.K.; Siri-Nguan, N.; Sornchamni, T.; Chareonpanich, M.; Kongkachuichay, P.; Yigit, N.; Rupprechter, G.; et al. Tuning Interactions of Surface-adsorbed Species over Fe-Co/K-Al₂O₃ Catalyst by Different K Contents: Selective CO₂ Hydrogenation to Light Olefins. *Chemcatchem* **2020**, *12*, 3306–3320. [[CrossRef](#)]
73. Dong, Z.C.; Zhao, J.; Tian, Y.J.; Zhang, B.F.; Wu, Y. Preparation and Performances of ZIF-67-Derived FeCo Bimetallic Catalysts for CO₂ Hydrogenation to Light Olefins. *Catalysts* **2020**, *10*, 455. [[CrossRef](#)]
74. Kim, K.Y.; Lee, H.; Noh, W.Y.; Shin, J.; Han, S.J.; Kim, S.K.; An, K.; Lee, J.S. Cobalt Ferrite Nanoparticles to Form a Catalytic Co-Fe Alloy Carbide Phase for Selective CO₂ Hydrogenation to Light Olefins. *ACS Catal.* **2020**, *10*, 8660–8671. [[CrossRef](#)]
75. Xu, Q.; Xu, X.; Fan, G.; Yang, L.; Li, F. Unveiling the roles of Fe-Co interactions over ternary spinel-type ZnCo_xFe_{2-x}O₄ catalysts for highly efficient CO₂ hydrogenation to produce light olefins. *J. Catal.* **2021**, *400*, 355–366. [[CrossRef](#)]
76. Zhang, J.; Su, X.; Wang, X.; Ma, Q.; Fan, S.; Zhao, T.S. Promotion effects of Ce added Fe-Zr-K on CO₂ hydrogenation to light olefins. *React. Kinet. Mech. Catal.* **2018**, *124*, 575–585. [[CrossRef](#)]
77. Wang, W.; Jiang, X.; Wang, X.; Song, C. Fe-Cu bimetallic catalysts for selective CO₂ hydrogenation to olefin-rich C₂₊ hydrocarbons. *Ind. Eng. Chem. Res.* **2018**, *57*, 4535–4542. [[CrossRef](#)]
78. Li, Z.; Wu, W.; Wang, M.; Wang, Y.; Ma, X.; Luo, L.; Chen, Y.; Fan, K.; Pan, Y.; Li, H.; et al. Ambient-pressure hydrogenation of CO₂ into long-chain olefins. *Nat. Commun.* **2022**, *13*, 2396. [[CrossRef](#)]
79. Liang, B.; Duan, H.; Sun, T.; Ma, J.; Liu, X.; Xu, J.; Su, X.; Huang, Y.; Zhang, T. Effect of Na promoter on Fe-based catalyst for CO₂ hydrogenation to alkenes. *ACS Sustain. Chem. Eng.* **2018**, *7*, 925–932. [[CrossRef](#)]
80. Visconti, C.G.; Martinelli, M.; Falbo, L.; Infantes-Molina, A.; Lietti, L.; Forzatti, P.; Iaquaniello, G.; Palo, E.; Picutti, B.; Brignoli, F. CO₂ hydrogenation to lower olefins on a high surface area K-promoted bulk Fe-catalyst. *Appl. Catal. B-Environ.* **2017**, *200*, 530–542. [[CrossRef](#)]
81. You, Z.Y.; Deng, W.P.; Zhang, Q.H.; Wang, Y. Hydrogenation of carbon dioxide to light olefins over non-supported iron catalyst. *Chin. J. Catal.* **2013**, *34*, 956–963. [[CrossRef](#)]
82. Gnanamani, M.K.; Hamdeh, H.H.; Shafer, W.D.; Hopps, S.D.; Davis, B.H. Hydrogenation of carbon dioxide over iron carbide prepared from alkali metal promoted iron oxalate. *Appl. Catal. A-Gen.* **2018**, *564*, 243–249. [[CrossRef](#)]
83. Jiang, F.; Liu, B.; Geng, S.; Xu, Y.; Liu, X. Hydrogenation of CO₂ into hydrocarbons: Enhanced catalytic activity over Fe-based Fischer-Tropsch catalysts. *Catal. Sci. Technol.* **2018**, *8*, 4097–4107. [[CrossRef](#)]
84. Yang, S.; Chun, H.-J.; Lee, S.; Han, S.J.; Lee, K.-Y.; Kim, Y.T. Comparative Study of Olefin Production from CO and CO₂ Using Na- and K-Promoted Zinc Ferrite. *ACS Catal.* **2020**, *10*, 10742–10759. [[CrossRef](#)]
85. Wang, X.; Wu, D.; Zhang, J.; Gao, X.; Ma, Q.; Fan, S.; Zhao, T.-S. Highly selective conversion of CO₂ to light olefins via Fischer-Tropsch synthesis over stable layered K-Fe-Ti catalysts. *Appl. Catal. A-Gen.* **2019**, *573*, 32–40. [[CrossRef](#)]
86. Zhang, J.; Lu, S.; Su, X.; Fan, S.; Ma, Q.; Zhao, T. Selective formation of light olefins from CO₂ hydrogenation over Fe-Zn-K catalysts. *J. CO₂ Util.* **2015**, *12*, 95–100. [[CrossRef](#)]
87. Dang, S.; Gao, P.; Liu, Z.; Chen, X.; Yang, C.; Wang, H.; Zhong, L.; Li, S.; Sun, Y. Role of zirconium in direct CO₂ hydrogenation to lower olefins on oxide/zeolite bifunctional catalysts. *J. Catal.* **2018**, *364*, 382–393. [[CrossRef](#)]
88. Gong, W.; Ye, R.-P.; Ding, J.; Wang, T.; Shi, X.; Russell, C.K.; Tang, J.; Eddings, E.G.; Zhang, Y.; Fan, M. Effect of copper on highly effective Fe-Mn based catalysts during production of light olefins via Fischer-Tropsch process with low CO₂ emission. *Appl. Catal. B-Environ.* **2020**, *278*, 119302. [[CrossRef](#)]
89. Ngantsoue-Hoc, W.; Zhang, Y.Q.; O'Brien, R.J.; Luo, M.S.; Davis, B.H. Fischer-Tropsch synthesis: Activity and selectivity for Group I alkali promoted iron-based catalysts. *Appl. Catal. A-Gen.* **2002**, *236*, 77–89. [[CrossRef](#)]
90. Wang, P.; Kang, J.; Zhang, Q.; Wang, Y. Lithium ion-exchanged zeolite faujasite as support of iron catalyst for Fischer-Tropsch synthesis. *Catal. Lett.* **2007**, *114*, 178–184. [[CrossRef](#)]
91. Yang, Q.; Kondratenko, V.A.; Petrov, S.A.; Doronkin, D.E.; Saraci, E.; Lund, H.; Arinchtein, A.; Kraehnert, R.; Skrypnik, A.S.; Matvienko, A.A.; et al. Identifying Performance Descriptors in CO₂ Hydrogenation over Iron-Based Catalysts Promoted with Alkali Metals. *Angew. Chem. Int. Ed.* **2022**, *61*, e202116517. [[CrossRef](#)]

92. Wang, S.; Ji, Y.; Liu, X.; Yan, S.; Xie, S.; Pei, Y.; Li, H.; Qiao, M.; Zong, B. Potassium as a Versatile Promoter to Tailor the Distribution of the Olefins in CO₂ Hydrogenation over Iron-Based Catalyst. *Chemcatchem* **2022**, *14*, e202101535. [[CrossRef](#)]
93. Jiang, M.; Koizumi, N.; Yamada, M. Characterization of potassium-promoted iron-manganese catalysts by insitu diffuse reflectance FTIR using NO, CO and CO+H₂ as probes. *Appl. Catal. A-Gen.* **2000**, *204*, 49–58. [[CrossRef](#)]
94. Tu, W.; Sun, C.; Zhang, Z.; Liu, W.; Malhi, H.S.; Ma, W.; Zhu, M.; Han, Y.-F. Chemical and structural properties of Na decorated Fe₅C₂-ZnO catalysts during hydrogenation of CO₂ to linear α -olefins. *Appl. Catal. B-Environ.* **2021**, *298*, 120567. [[CrossRef](#)]
95. Witoon, T.; Chaipraditgul, N.; Numpilai, T.; Lapkeatseree, V.; Ayodele, B.V.; Cheng, C.K.; Siri-Nguan, N.; Sornchamni, T.; Limtrakul, J. Highly active Fe-Co-Zn/K-Al₂O₃ catalysts for CO₂ hydrogenation to light olefins. *Chem. Eng. Sci.* **2021**, *233*, 116428. [[CrossRef](#)]
96. Hwang, S.M.; Han, S.J.; Min, J.E.; Park, H.G.; Jun, K.W.; Kim, S.K. Mechanistic insights into Cu and K promoted Fe-catalyzed production of liquid hydrocarbons via CO₂ hydrogenation. *J. CO₂ Util.* **2019**, *34*, 522–532. [[CrossRef](#)]
97. Chaipraditgul, N.; Numpilai, T.; Cheng, C.K.; Siri-Nguan, N.; Sornchamni, T.; Wattanakit, C.; Limtrakul, J.; Witoon, T. Tuning interaction of surface-adsorbed species over Fe/K-Al₂O₃ modified with transition metals (Cu, Mn, V, Zn or Co) on light olefins production from CO₂ hydrogenation. *Fuel* **2021**, *283*, 119248. [[CrossRef](#)]
98. Chen, Y.; Li, X.; Zhang, J.; Zhao, N.; Dai, L.; Jiang, X.; Liu, C.; Lyu, S.; Li, Z. Preparation of SiO₂ immobilized Co-based catalysts from ZIF-67 and the enhancement effect for Fischer-Tropsch synthesis. *Appl. Catal. B-Environ.* **2021**, *289*, 120027. [[CrossRef](#)]
99. Li, X.; Chen, Y.; Nisa, M.U.; Li, Z. Combating poison with poison—Irreducible Co₂SiO₄ as a promoter to modify Co-based catalysts in Fischer-Tropsch synthesis. *Appl. Catal. B-Environ.* **2020**, *267*, 118377. [[CrossRef](#)]
100. Duvenhage, D.J.; Coville, N.J. Fe:Co/TiO₂ bimetallic catalysts for the Fischer-Tropsch reaction I. Characterization and reactor studies. *Appl. Catal. A-Gen.* **1997**, *153*, 43–67. [[CrossRef](#)]
101. Li, T.; Yang, Y.; Zhang, C.; An, X.; Wan, H.; Tao, Z.; Xiang, H.; Li, Y.; Yi, F.; Xu, B. Effect of manganese on an iron-based Fischer-Tropsch synthesis catalyst prepared from ferrous sulfate. *Fuel* **2007**, *86*, 921–928. [[CrossRef](#)]
102. Zhang, Z.P.; Dai, W.W.; Xu, X.C.; Zhang, J.; Shi, B.F.; Xu, J.; Tu, W.F.; Han, Y.F. MnO_x promotional effects on olefins synthesis directly from syngas over bimetallic Fe-MnO_x/SiO₂ catalysts. *AIChE J.* **2017**, *63*, 4451–4464. [[CrossRef](#)]
103. Kuci, C.-K.; Chen, W.-S.; Lee, M.-D. Hydrogenation of Carbon Dioxide on Iron Manganese Catalysts. *J. Chin. Chem. Soc.* **1991**, *38*, 127–139. [[CrossRef](#)]
104. Nie, X.; Wang, H.; Janik, M.J.; Chen, Y.; Guo, X.; Song, C. Mechanistic Insight into C-C Coupling over Fe-Cu Bimetallic Catalysts in CO₂ Hydrogenation. *J. Phys. Chem. C* **2017**, *121*, 13164–13174. [[CrossRef](#)]
105. Nie, X.; Wang, H.; Janik, M.J.; Guo, X.; Song, C. Computational Investigation of Fe-Cu Bimetallic Catalysts for CO₂ Hydrogenation. *J. Phys. Chem. C* **2016**, *120*, 9364–9373. [[CrossRef](#)]
106. Zhang, C.; Cao, C.; Zhang, Y.; Liu, X.; Xu, J.; Zhu, M.; Tu, W.; Han, Y.-F. Unraveling the Role of Zinc on Bimetallic Fe₅C₂-ZnO Catalysts for Highly Selective Carbon Dioxide Hydrogenation to High Carbon α -Olefins. *ACS Catal.* **2021**, *11*, 2121–2133. [[CrossRef](#)]
107. Daelman, N.; Capdevila-Cortada, M.; López, N. Dynamic charge and oxidation state of Pt/CeO₂ single-atom catalysts. *Nat. Mater.* **2019**, *18*, 1215–1221. [[CrossRef](#)]
108. Tang, H.; Su, Y.; Zhang, B.; Lee, A.F.; Isaacs, M.A.; Wilson, K.; Li, L.; Ren, Y.; Huang, J.; Haruta, M.; et al. Classical strong metal-support interactions between gold nanoparticles and titanium dioxide. *Sci. Adv.* **2017**, *3*, e1700231. [[CrossRef](#)]
109. Parastaev, A.; Muravev, V.; Huertas Osta, E.; van Hoof, A.J.F.; Kimpel, T.F.; Kosinov, N.; Hensen, E.J.M. Boosting CO₂ hydrogenation via size-dependent metal-support interactions in cobalt/ceria-based catalysts. *Nat. Catal.* **2020**, *3*, 526–533. [[CrossRef](#)]
110. Divin, N.J.; Angurell, I.; Escudero, C.; Perez-Dieste, V.; Llorca, J. Influence of the support on surface rearrangements of bimetallic nanoparticles in real catalysts. *Science* **2014**, *346*, 620–623. [[CrossRef](#)]
111. Fu, Q.; Saltsburg, H.; Flytzani-Stephanopoulos, M. Active nonmetallic Au and Pt species on ceria-based water-gas shift catalysts. *Science* **2003**, *301*, 935–938. [[CrossRef](#)]
112. Pandey, D.; Deo, G. Promotional effects in alumina and silica supported bimetallic Ni-Fe catalysts during CO₂ hydrogenation. *J. Mol. Catal. A Chem.* **2014**, *382*, 23–30. [[CrossRef](#)]
113. Ding, J.; Zhao, W.X.; Zi, L.T.; Xu, X.; Liu, Q.; Zhong, Q.; Xu, Y. Promotional Effect of ZrO₂ on supported FeCoK Catalysts for Ethylene Synthesis from catalytic CO₂ hydrogenation. *Int. J. Hydrogen Energy* **2020**, *45*, 15254–15262. [[CrossRef](#)]
114. Chernyak, S.A.; Ivanov, A.S.; Stolbov, D.N.; Maksimov, S.V.; Maslakov, K.I.; Chernavskii, P.A.; Pokusaeva, Y.A.; Koklin, A.E.; Bogdan, V.I.; Savilov, S.V. Sintered Fe/CNT framework catalysts for CO₂ hydrogenation into hydrocarbons. *Carbon* **2020**, *168*, 475–484. [[CrossRef](#)]
115. Lee, H.J.; Cho, W.; Lim, E.; Oh, M. One-pot synthesis of magnetic particle-embedded porous carbon composites from metal-organic frameworks and their sorption properties. *Chem. Commun.* **2014**, *50*, 5476–5479. [[CrossRef](#)] [[PubMed](#)]
116. Wezendonk, T.A.; Santos, V.P.; Nasalevich, M.A.; Warringa, Q.S.E.; Dugulan, A.I.; Chojecki, A.; Koeken, A.C.J.; Ruitenbeek, M.; Meima, G.; Islam, H.-U.; et al. Elucidating the Nature of Fe Species during Pyrolysis of the Fe-BTC MOF into Highly Active and Stable Fischer-Tropsch Catalysts. *ACS Catal.* **2016**, *6*, 3236–3247. [[CrossRef](#)]
117. Liu, J.; Sun, Y.; Jiang, X.; Zhang, A.; Song, C.; Guo, X. Pyrolyzing ZIF-8 to N-doped porous carbon facilitated by iron and potassium for CO₂ hydrogenation to value-added hydrocarbons. *J. CO₂ Util.* **2018**, *25*, 120–127. [[CrossRef](#)]

118. Liu, J.; Zhang, A.; Jiang, X.; Zhang, G.; Sun, Y.; Liu, M.; Ding, F.; Song, C.; Guo, X. Overcoating the Surface of Fe-Based Catalyst with ZnO and Nitrogen-Doped Carbon toward High Selectivity of Light Olefins in CO₂ Hydrogenation. *Ind. Eng. Chem. Res.* **2019**, *58*, 4017–4023. [[CrossRef](#)]
119. Liu, J.; Zhang, A.; Liu, M.; Hu, S.; Ding, F.; Song, C.; Guo, X. Fe-MOF-derived highly active catalysts for carbon dioxide hydrogenation to valuable hydrocarbons. *J. CO₂ Util.* **2017**, *21*, 100–107. [[CrossRef](#)]
120. An, B.; Cheng, K.; Wang, C.; Wang, Y.; Lin, W. Pyrolysis of Metal-Organic Frameworks to Fe₃O₄@Fe₅C₂ Core-Shell Nanoparticles for Fischer-Tropsch Synthesis. *ACS Catal.* **2016**, *6*, 3610–3618. [[CrossRef](#)]
121. Wang, X.; Yang, G.; Zhang, J.; Chen, S.; Wu, Y.; Zhang, Q.; Wang, J.; Han, Y.; Tan, Y. Synthesis of isoalkanes over a core (Fe–Zn–Zr)–shell (zeolite) catalyst by CO₂ hydrogenation. *Chem. Commun.* **2016**, *52*, 7352–7355. [[CrossRef](#)]
122. Roque-Malherbe, R.M.A.; Wendelbo, R.; Mifsud, A.; Corma, A.J.T.J.o.P.C. Diffusion of aromatic hydrocarbons in H-ZSM-5, H-Beta, and H-MCM-22 zeolites. *J. Phys. Chem.* **1995**, *99*, 14064–14071. [[CrossRef](#)]
123. Chen, J.; Liang, T.; Li, J.; Wang, S.; Qin, Z.; Wang, P.; Huang, L.; Fan, W.; Wang, J. Regulation of Framework Aluminum Siting and Acid Distribution in H-MCM-22 by Boron Incorporation and Its Effect on the Catalytic Performance in Methanol to Hydrocarbons. *ACS Catal.* **2016**, *6*, 2299–2313. [[CrossRef](#)]
124. Grabowska, E. Selected perovskite oxides: Characterization, preparation and photocatalytic properties—A review. *Appl. Catal. B-Environ.* **2016**, *186*, 97–126. [[CrossRef](#)]
125. Yang, Q.; Liu, G.; Liu, Y. Perovskite-Type Oxides as the Catalyst Precursors for Preparing Supported Metallic Nanocatalysts: A Review. *Ind. Eng. Chem. Res.* **2018**, *57*, 1–17. [[CrossRef](#)]
126. Tejuca, L.G.; Fierro, J.L.G.; Tascón, J.M.D. Structure and Reactivity of Perovskite-Type Oxides. In *Advances in Catalysis*; Eley, D.D., Pines, H., Weisz, P.B., Eds.; Academic Press: Cambridge, MA, USA, 1989; Volume 36.
127. Ren, J.; Mebrahtu, C.; van Koppen, L.; Martinovic, F.; Hofmann, J.P.; Hensen, E.J.M.; Palkovits, R. Enhanced CO₂ methanation activity over La_{2-x}Ce_xNiO₄ perovskite-derived catalysts: Understanding the structure-performance relationships. *Chem. Eng. J.* **2021**, *426*, 131760. [[CrossRef](#)]
128. Bedel, L.; Roger, A.-C.; Rehspringer, J.-L.; Zimmermann, Y.; Kiennemann, A. La_(1-y)Co_{0.4}Fe_{0.6}O_{3-δ} perovskite oxides as catalysts for Fischer-Tropsch synthesis. *J. Catal.* **2005**, *235*, 279–294. [[CrossRef](#)]
129. Ma, L.-H.; Gao, X.-H.; Ma, J.-J.; Hu, X.-D.; Zhang, J.-L.; Guo, Q.-J. K/LaFeMnO₃ Perovskite-Type Oxide Catalyst for the Production of C₂–C₄ Olefins via CO Hydrogenation. *Catal. Lett.* **2022**, *152*, 1451–1460. [[CrossRef](#)]
130. Liu, Z.; Jia, G.; Zhao, C.; Xing, Y. Selective Iron Catalysts for Direct Fischer-Tropsch Synthesis to Light Olefins. *Ind. Eng. Chem. Res.* **2021**, *60*, 6137–6146. [[CrossRef](#)]
131. Ao, M.; Pham, G.H.; Sage, V.; Pareek, V.; Liu, S. Perovskite-derived trimetallic Co-Ni-Cu catalyst for higher alcohol synthesis from syngas. *Fuel Process. Technol.* **2019**, *193*, 141–148. [[CrossRef](#)]
132. Daza, Y.A.; Kent, R.A.; Yung, M.M.; Kuhn, J.N. Carbon Dioxide Conversion by Reverse Water-Gas Shift Chemical Looping on Perovskite-Type Oxides. *Ind. Eng. Chem. Res.* **2014**, *53*, 5828–5837. [[CrossRef](#)]
133. Lindenthal, L.; Popovic, J.; Rameshan, R.; Huber, J.; Schrenk, F.; Ruh, T.; Nenning, A.; Löffler, S.; Opitz, A.K.; Rameshan, C. Novel perovskite catalysts for CO₂ utilization - Exsolution enhanced reverse water-gas shift activity. *Appl. Catal. B-Environ.* **2021**, *292*, 120183. [[CrossRef](#)]
134. Utsis, N.; Vidruk-Nehemya, R.; Landau, M.V.; Herskowitz, M. Novel bifunctional catalysts based on crystalline multi-oxide matrices containing iron ions for CO₂ hydrogenation to liquid fuels and chemicals. *Faraday Discuss.* **2016**, *188*, 545–563. [[CrossRef](#)]
135. Hou, Y.; Wang, X.; Chen, M.; Gao, X.; Liu, Y.; Guo, Q. Sr_{1-x}K_xFeO₃ Perovskite Catalysts with Enhanced RWGS Reactivity for CO₂ Hydrogenation to Light Olefins. *Atmosphere* **2022**, *13*, 760. [[CrossRef](#)]
136. Kwak, J.H.; Kovarik, L.; Szanyi, J. CO₂ Reduction on Supported Ru/Al₂O₃ Catalysts: Cluster Size Dependence of Product Selectivity. *ACS Catal.* **2013**, *3*, 2449–2455. [[CrossRef](#)]
137. Xie, T.; Wang, J.; Ding, F.; Zhang, A.; Li, W.; Guo, X.; Song, C. CO₂ hydrogenation to hydrocarbons over alumina-supported iron catalyst: Effect of support pore size. *J. CO₂ Util.* **2017**, *19*, 202–208. [[CrossRef](#)]
138. Wu, H.C.; Chang, Y.C.; Wu, J.H.; Lin, J.H.; Lin, I.K.; Chen, C.S. Methanation of CO₂ and reverse water gas shift reactions on Ni/SiO₂ catalysts: The influence of particle size on selectivity and reaction pathway. *Catal. Sci. Technol.* **2015**, *5*, 4154–4163. [[CrossRef](#)]
139. Iablokov, V.; Beaumont, S.K.; Alayoglu, S.; Pushkarev, V.V.; Specht, C.; Gao, J.; Alivisatos, A.P.; Kruse, N.; Somorjai, G.A. Size-Controlled Model Co Nanoparticle Catalysts for CO₂ Hydrogenation: Synthesis, Characterization, and Catalytic Reactions. *Nano Lett.* **2012**, *12*, 3091–3096. [[CrossRef](#)] [[PubMed](#)]
140. Hong, J.S.; Hwang, J.S.; Jun, K.W.; Sur, J.C.; Lee, K.W. Deactivation study on a coprecipitated Fe-Cu-K-Al catalyst in CO₂ hydrogenation. *Appl. Catal. A-Gen.* **2001**, *218*, 53–59. [[CrossRef](#)]
141. Zhu, J.; Zhang, G.; Li, W.; Zhang, X.; Ding, F.; Song, C.; Guo, X. Deconvolution of the Particle Size Effect on CO₂ Hydrogenation over Iron-Based Catalysts. *ACS Catal.* **2020**, *10*, 7424–7433. [[CrossRef](#)]
142. Podgurski, H.; Kummer, J.; DeWitt, T.; Emmett, P. Preparation, Stability and Adsorptive Properties of the Carbides of Iron. *J. Am. Chem. Soc.* **1950**, *72*, 5382–5388. [[CrossRef](#)]
143. Brady, R.C.; Pettit, R. On the Mechanism of the Fischer-Tropsch reaction. The chain propagation step. *J. Am. Chem. Soc.* **1981**, *103*, 1287–1289. [[CrossRef](#)]

144. Chuang, S.; Tian, Y.; Goodwin Jr, J.; Wender, I. The use of probe molecules in the study of CO hydrogenation over SiO₂-supported Ni, Ru, Rh, and Pd. *J. Catal.* **1985**, *96*, 396–407. [[CrossRef](#)]
145. Riedel, T.; Schulz, H.; Schaub, G.; Jun, K.W.; Hwang, J.S.; Lee, K.W. Fischer-Tropsch on iron with H₂/CO and H₂/CO₂ as synthesis gases: The episodes of formation of the Fischer-Tropsch regime and construction of the catalyst. *Top. Catal.* **2003**, *26*, 41–54. [[CrossRef](#)]
146. Puga, A.V. On the nature of active phases and sites in CO and CO₂ hydrogenation catalysts. *Catal. Sci. Technol.* **2018**, *8*, 5681–5707. [[CrossRef](#)]
147. Han, S.J.; Hwang, S.-M.; Park, H.-G.; Zhang, C.; Jun, K.-W.; Kim, S.K. Identification of active sites for CO₂ hydrogenation in Fe catalysts by first-principles microkinetic modelling. *J. Mater. Chem. A* **2020**, *8*, 13014–13023. [[CrossRef](#)]
148. Wang, H.; Nie, X.; Liu, Y.; Janik, M.J.; Han, X.; Deng, Y.; Hu, W.; Song, C.; Guo, X. Mechanistic Insight into Hydrocarbon Synthesis via CO₂ Hydrogenation on χ -Fe₅C₂ Catalysts. *ACS Appl. Mater. Interfaces* **2022**, *14*, 37637–37651. [[CrossRef](#)] [[PubMed](#)]
149. Cui, X.; Gao, P.; Li, S.; Yang, C.; Liu, Z.; Wang, H.; Zhong, L.; Sun, Y. Selective Production of Aromatics Directly from Carbon Dioxide Hydrogenation. *ACS Catal.* **2019**, *9*, 3866–3876. [[CrossRef](#)]
150. Bukur, D.B.; Okabe, K.; Rosynek, M.P.; Li, C.P.; Wang, D.J.; Rao, K.R.P.M.; Huffman, G.P. Activation Studies with a Precipitated Iron Catalyst for Fischer-Tropsch Synthesis: I. Characterization Studies. *J. Catal.* **1995**, *155*, 353–365. [[CrossRef](#)]
151. Raupp, G.B.; Delgass, W.N. Mössbauer investigation of supported Fe and FeNi catalysts: II. Carbides formed Fischer-Tropsch synthesis. *J. Catal.* **1979**, *58*, 348–360. [[CrossRef](#)]
152. de Smit, E.; Cinquini, F.; Beale, A.M.; Safonova, O.V.; van Beek, W.; Sautet, P.; Weckhuysen, B.M. Stability and Reactivity of epsilon-chi-theta Iron Carbide Catalyst Phases in Fischer-Tropsch Synthesis: Controlling $\mu(c)$. *J. Am. Chem. Soc.* **2010**, *132*, 14928–14941. [[CrossRef](#)]
153. Mazzucco, S.; Wang, Y.; Tanase, M.; Picher, M.; Li, K.; Wu, Z.; Irle, S.; Sharma, R. Direct evidence of active and inactive phases of Fe catalyst nanoparticles for carbon nanotube formation. *J. Catal.* **2014**, *319*, 54–60. [[CrossRef](#)]
154. Yang, X.; Zhang, H.; Liu, Y.; Ning, W.; Han, W.; Liu, H.; Huo, C. Preparation of Iron Carbides Formed by Iron Oxalate Carburization for Fischer-Tropsch Synthesis. *Catalysts* **2019**, *9*, 347. [[CrossRef](#)]